

2024

Characterization of a Single Bladed Propeller used for Actuating an Autonomous Undersea Vehicle

Donald Samuel Alexander
University of Rhode Island, dsalexander68@gmail.com

Follow this and additional works at: <https://digitalcommons.uri.edu/theses>

Recommended Citation

Alexander, Donald Samuel, "Characterization of a Single Bladed Propeller used for Actuating an Autonomous Undersea Vehicle" (2024). *Open Access Master's Theses*. Paper 2460.
<https://digitalcommons.uri.edu/theses/2460>

This Thesis is brought to you by the University of Rhode Island. It has been accepted for inclusion in Open Access Master's Theses by an authorized administrator of DigitalCommons@URI. For more information, please contact digitalcommons-group@uri.edu. For permission to reuse copyrighted content, contact the author directly.

CHARACTERIZATION OF A SINGLE BLADED
PROPELLER USED FOR ACTUATING AN
AUTONOMOUS UNDERSEA VEHICLE
BY
DONALD SAMUEL ALEXANDER

A THESIS SUBMITTED IN PARTIAL FULFILLMENT OF THE
REQUIREMENTS FOR THE DEGREE OF
MASTER OF SCIENCE
IN
OCEAN ENGINEERING

UNIVERSITY OF RHODE ISLAND

2024

MASTER OF SCIENCE THESIS
OF
DONALD SAMUEL ALEXANDER

APPROVED:

Thesis Committee:

Major Professor Stephen Licht

Brennan Phillips

Mingxi Zhou

Brenton DeBoef
DEAN OF THE GRADUATE SCHOOL

UNIVERSITY OF RHODE ISLAND
2024

ABSTRACT

An asymmetric propulsion design using a single bladed propeller is proposed as a viable method for an Unmanned Undersea Vehicle (UUV) to obtain maneuvering capability in all 6 Degrees of Freedom (DOF) with a single actuator. This substantially reduces the complexity of the UUV while enabling it to perform missions which could be assigned to an Autonomous Undersea Vehicle (AUV). Existing AUV actuator designs are very complex to implement for most research applications. Current UUV architecture is either optimized for long endurance survey missions as AUVs or precise maneuvering as tethered ROVs. Both versions require several actuators to provide maneuvering capability in all 6 DOF.

Previous literature is focused on assessing the viability of the single bladed propeller. However, little work has been done to develop a design methodology for the single bladed propeller or compare the viability of this propulsion system to a conventionally actuated AUV. This thesis seeks to close this gap by developing a dynamic simulation model for the single bladed propeller actuated AUV and comparing its performance against a similar AUV actuated by conventional fins and stern planes. A single bladed propeller actuated AUV is shown to provide similar performance to a conventionally actuated AUV while commanded to conduct large course and depth changes. However, additional design and operational consideration must be applied to the single bladed propeller to maximize its maneuvering potential.

ACKNOWLEDGMENTS

I would like to thank Jesus Christ for the grace He has given me. My fiancée Alyssa, for her love and support through this process. My parents for their love and support throughout my life. Professor Licht and Professor Miller for mentoring me and teaching me the tools and tactics necessary for conducting this research. CAPT Quintin James USN, CAPT Sean Gray USN, CDR Chad Guillerault USN, CDR Matthew Powell USN, CDR John Coleman III USN, CDR Kevin O'Malley USN, LCDR Chris Dematteo USN, LCDR Bradley Harden USN, LCDR Peter Alexakos USN, and the wardrooms of USS IOWA (SSN 797) and Undersea Warfighting Development Center for their support through duty day rotations, recommendations, and work day support to accomplish this goal. Finally, thanks to the Officer Christian Fellowship Cadets and ministry at the US Coast Guard Academy for the support, antics, and love they have shown during this period.

Table of Contents

ABSTRACT	ii
ACKNOWLEDGEMENTS	iii
TABLE OF CONTENTS	iv
LIST OF TABLES	vii
LIST OF FIGURES	viii
Chapter 1 Introduction	1
1.1 Project motivation	1
1.2 Proposed design methodology	2
Chapter 2 Background	4
2.1 UUV applications	4
2.2 UUV control architecture	6
2.2.1 Conventional AUV control design	6
2.3 AUV cost considerations and limitations	6
2.4 Prior work on single bladed propellers	7
2.5 Single bladed propeller benefit	8
2.6 Control system architecture	8
2.7 Applications and summary	9
Chapter 3 Design Case Study	11
3.1 Introduction	11
3.2 Modeling and simulation approach	13
3.2.1 Coordinate system	13
3.2.2 Rigid body equations of motion	14
3.2.3 Hydrodynamic coefficient development	16
3.2.3.1 Hull profile calculation	16
3.2.3.2 Strip theory	20
3.2.3.3 Prolate spheroid approximation	22

3.2.3.4 Control surface force coefficient calculation	23
3.2.4 Model linearization.....	26
3.2.4.1 Linearized time invariant system.....	26
3.2.4.2 Sway-yaw model	27
3.2.4.3 Pitch-heave model	29
3.2.4.4 Surge velocity model	30
3.2.5.4 Coupled controller model.....	30
3.2.5 Single bladed propeller thrust and torque characterization.....	31
3.3 MATLAB/SIMULINK implementation.....	33
3.4 Applying the propeller sizing procedure.....	33
3.4.1 Determine propeller RPM as a function of blade length for design maximum speeds	34
3.4.2 Model advance, transfer, tactical diameter, and depth changing performance as a function of speed and propeller diameter	36
3.4.2.1 Course changing open loop tests	36
3.4.2.2 Depth changing open loop tests	37
3.4.2.3 Angular velocity differential tests	38
3.4.2.4 Composite control tests	38
3.5 Data Analysis	39
3.6 Comparison model.....	40
Chapter 4 Results.....	42
4.1 Results of the propeller sizing procedure.....	42
4.1.1 Determine propeller RPM as a function of blade length for design maximum speeds	42
4.1.2 Model advance, transfer, tactical diameter, and depth changing performance as a function of speed and propeller diameter	44
4.1.2.1 Modeling advance, transfer, and tactical diameter	44
4.1.2.2 Modeling depth changing performance	46
4.1.2.3 Propeller angular velocity differential tests	48
4.1.2.4 Coupled maneuvering dynamic test	48
4.1.2.5 Coupled controller performance degradation	51

4.1.2.6 Operating region and propeller blade size	53
4.2 Based on the Modeling and Simulation results select the optimum propeller blade length to meet design requirements	55
4.3 Additional Results	57
4.3.1 Single bladed propeller vs. rudder performance.....	57
4.3.2 Shroud effectiveness	58
4.4 Identified limitations.....	61
Chapter 5 Discussion and Future Work	62
5.1 Design Methodology	62
5.1.1 Design Considerations	62
5.1.2 Limitation Mitigation.....	63
5.2 Recommendations for Future Work	64
5.2.1 Physical Model Verification	64
5.2.2 Roll Susceptibility Analysis.....	65
5.2.3 Path Following Capability Analysis	65
5.2.4 Long Term Pitch Control	66
5.2.5 Control Authority Allocation and Prioritization	68
Appendices	69
Appendix A. Mass Matrix Data	69
Appendix B. Hydrodynamic and Damping Coefficients	71
Appendix C. Course changing open loop test data	72
Appendix D. Depth changing open loop test data	83
Appendix E. Surge Velocity changing open loop test data	89
Appendix F. Coupled Controller Analysis Data	95
Bibliography.....	102

LIST OF TABLES

TABLE	PAGE
Table 3-1 Short-Hulled AUV design characteristics.....	12
Table 3-2: Modeling and simulation assumptions	13
Table 3-3: Sway yaw PID controller coefficients.....	29
Table 3-4: Pitch heave PID controller coefficients.....	30
Table 3-5 Retained data.....	40
Table 3-6 Rudder sway yaw PID controller coefficients	41
Table 3-7 Fin pitch-heave PID controller coefficients.....	41
Table 4-1: Surge velocity to propeller rpm equations.....	43
Table 4-2: Test case description.....	50
Table 4-3: Course changing performance degradation	51
Table 4-4: Shroud impact on maximum surge velocity	59
Table 4-5: Change in UUV maneuvering performance at 1.5 m/s based on incorporation of the shroud	60

LIST OF FIGURES

FIGURE	PAGE
Figure 2-1: ROV example.....	4
Figure 2-2: REMUS 620 AUV example	5
Figure 2-3: Example of a single bladed propeller	7
Figure 2-4: Example of single bladed propeller moment generation	8
Figure 2-5: Closed loop feedback loop	9
Figure 3-1: Short Hulled AUV.....	11
Figure 3-2: Short Hulled AUV measurement diagram.	12
Figure 3-3: Body fixed coordinate system	14
Figure 3-4: Prolate spheroid overlaid over a myring hull profile.....	17
Figure 3-5: Conventional test shape (upper left), conventional prolate spheroid (upper right), single bladed test shape (lower left), and single bladed prolate spheroid (lower right).....	19
Figure 3-6: Dimensions for a pair of identically sized control fins (left), Coefficient of additional moment of inertia for a flat plate (right).....	23
Figure 3-7: Steering angle and propeller orientation relationship.....	25
Figure 3-8: Steering angle applied to a decoupled course controller	26
Figure 3-9: Careli open water propeller performance curves.....	32
Figure 3-10: Surge velocity vs. propeller RPM example.....	35
Figure 3-11: Maneuvering characteristics example.....	37
Figure 3-12: Operating envelope example.....	40
Figure 4-1: Surge velocity vs. propeller RPM for the short hulled test shape	43

Figure	Page
Figure 4-2: Ideal turning speed.....	45
Figure 4-3: Maneuvering characteristics vs. propeller blade size	45
Figure 4-4: Turning time vs. propeller blade size.....	46
Figure 4-5: Depth overshoot vs. propeller blade size	47
Figure 4-6: Depth change time vs. propeller blade size.....	47
Figure 4-7: Maneuvering characteristics vs angular velocity difference	48
Figure 4-8: AUV maneuvering curves: case 1(upper left), case 2 (upper right), case 3 (lower left), case 4 (lower right).....	50
Figure 4-9: Case 1-4 overlaid plots (right), Rudder and Propeller No Speed Control overlaid (left).....	52
Figure 4-10: Turn time vs. surge velocity	54
Figure 4-11: Short hulled AUV operating envelope	57
Figure 4-12: Impact of the propeller shroud on surge velocity performance.....	59
Figure 4-13: Turn time vs. surge velocity comparing shrouded and unshrouded short hulled UUV performance	60
Figure 5-1: Example path following test.....	66
Figure 5-2: Depth control oscillation example.....	67

CHAPTER 1

INTRODUCTION

1.1 Project motivation:

The potential for UUVs is vast for all undersea applications despite their various engineering challenges. The two most mature forms, ROVs and AUVs, have been under development for several decades. Key engineering concerns include design complexity, cost, and endurance. This thesis will focus on applying a single bladed propeller as a propulsion method for an AUV. AUVs are typically designed as fully actuated or overactuated systems using a complex combination of thrusters, variable buoyancy, fins, and propellers for control in 6 DOF [14]. The large number of actuators results in an inherently complex system requiring a complex control architecture to operate. Even the most basic AUV designs requires either one or two thrusters coupled with control fins and a rudder. A novel propulsion concept is under development to use one single bladed propeller to actuate an AUV in 6 DOF [4], [10], [11].

Kaeli, Littlefield, Jaffre, and Carelli have demonstrated an asymmetric single bladed propeller can provide both forward propulsion, a yaw moment, and a pitch moment to effectively control the speed, course, and depth of an AUV [4], [10], [11]. This thesis develops the design criteria associated with an asymmetric propeller through modeling and simulation. A single bladed propeller can provide acceptable but reduced maneuvering performance compared to a conventional rudder and control fins. However, careful consideration must be given to prioritizing actuator output between course, depth, or speed control for a given task.

1.2 Proposed design methodology

The following design process is proposed to aid in determining propeller size for a given AUV configuration and propeller shape:

1. **Determine the AUV hull constraints and requirements.** The hull diameter may determine the maximum propeller blade size and preclude oversizing the propeller to improve maneuvering performance. If the hull diameter is not the limiting factor, then it provides a starting point for propeller sizing.
2. **Determine the design speed for the AUV sensors.** Ideally, the AUV will be designed to where its “optimum operating region” encompasses the optimum sensor speed.
3. **Determine the maximum required speed for the AUV.** This will ultimately determine the minimum propeller blade size. A propeller blade which is too small cannot provide enough thrust to maintain its desired surge velocity.
4. **Select basic propeller geometry (e.g. K_T , K_Q)**
5. **Propeller Sizing Procedure**
 - a. **Determine propeller RPM as a function of blade length for design maximum speeds.** This test assesses the capability of the single bladed propeller to provide the required maximum forward speed. A byproduct of this analysis is the relationship between the propeller RPM and surge velocity for use in follow on analysis.

b. Model advance, transfer, tactical diameter, and depth changing performance as a function of speed and propeller diameter.

This will include tests to determine the uncoupled and coupled vehicle dynamics maneuvering tests. The uncoupled tests will determine the absolute best and worst maneuvering capability to compare to conventional AUV performance. The coupled tests provide the actual operating region for AUV performance and assess whether it can meet mission requirements.

- 6. Based on the modeling and simulation results select the optimum propeller blade length to meet design requirements.** The optimum propeller blade length should be considered the largest blade size the AUV can use while meeting the AUV size requirements and power requirements. A larger propeller blade length substantially improves performance but can result in an AUV but subsequently increases the torque resisting the propeller's motion reducing efficiency. A motor may not be able to achieve the design maximum propeller RPM with a larger propeller blade due to the increased torque. Another concern is the size of the propeller blade length may result in an AUV design which is unwieldy for transport, storage, or preclude incorporation of thrust enhancing nozzles or shrouds.
- 7. Select the drive motor to provide the desired performance of the single bladed propeller.**

CHAPTER 2

BACKGROUND

2.1 UUV applications

Unmanned Undersea Vehicles (UUVs) have been an emerging technology for the past few decades. Their chief advantage is their ability to perform the functions of a manned submersible at extreme depths without risking the crews. This greatly reduces the risk and cost associated with undersea applications but invites a host of the engineering challenges associated with developing an autonomous system.

The most common UUVs are ROVs [14] as depicted in Figure 2-1. ROVs are designed to operate freely but require a tether to a mother ship, typically a surface vessel or manned submersible. ROVs are ideal for applications which require a precise positioning at slow speeds, i.e. Explosive Ordnance Disposal of naval mines, seabed oil drilling equipment repair, or shipwreck exploration. However, ROVs are dependent on their host ship/submersible for transit as their range is restricted to the length of their tether. In addition, their design is not optimized for efficient long range travel.

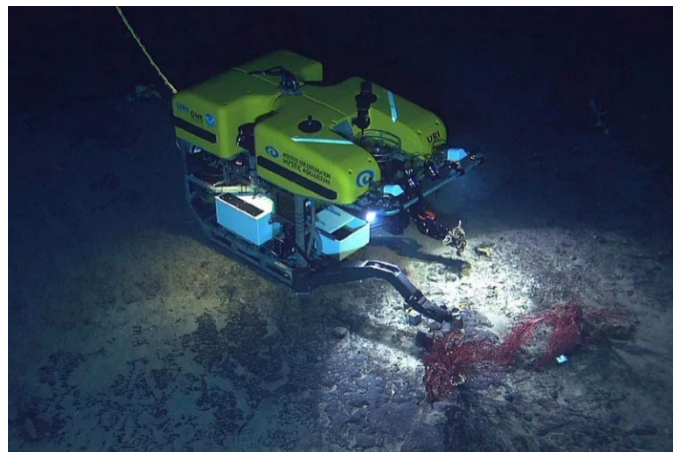


Figure 2-1: ROV example [22]

Another form of UUV is the AUV. AUVs share the torpedo like shape of a manned submarine as depicted in Figure 2-2. AUVs are designed as independent, tetherless underwater robots. Their torpedo like hull configuration [14] permits efficient long range transit at higher speeds than an ROV. This makes the AUV ideal for missions such as undersea imagery and survey using side scan and multibeam sonars. AUVs often use traditional undersea vehicle control surfaces such as a rudder and fins permitting depth and pitch control via inducing a yaw and pitch moment. This is sufficient for long range transit but cannot provide the precise dynamic positioning required for ROV operations. The rudder and fins require water flow along their span to produce a yaw or pitch moment which precludes low speed maneuvering. In addition, the lack of a tether requires the AUV to utilize a battery for power which limits mission time and requires optimized efficiency to maximize mission endurance. In both the ROV and AUV design, there is substantial mechanical complexity due to the large number of actuators increasing the maintenance and development required by the UUV designer and operator.

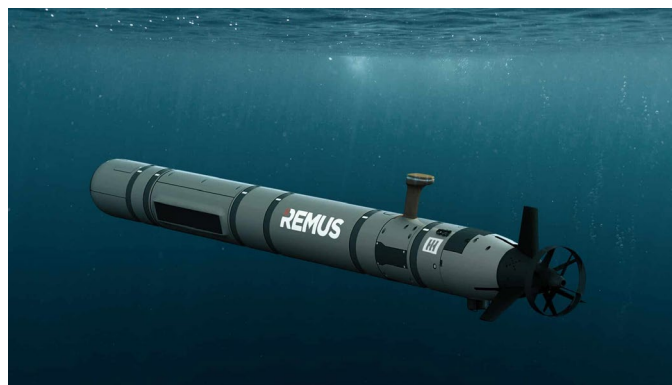


Figure 2-2: REMUS 620 AUV example [13]

2.2 AUV control architecture

An AUV requires actuation in multiple degrees of freedom. It must be able to simultaneously control course, speed, and depth either directly through thrusters or indirectly through use of pitch and yaw moments via control fins. The succeeding sections provides an overview of the control architecture of an AUV.

2.2.1 Conventional AUV control design

At its most basic form, an AUV is an underactuated system where the number of actuators is less than the total number of DOF of the AUV system. A conventional AUV will use a combination of the propeller coupled with a rudder and fins generate yaw and pitch moments to actuate course and depth changes. Newer designs may incorporate a thruster within the hull of the AUV to generate heave and sway velocity. However, the additional actuators substantially increase cost and complexity.

The incorporation of the rudder and fins allows for course and depth control to be treated as decoupled dynamic systems at the slow speeds (< 5 m/s) used by an AUV. This permits the use of decoupled Proportional-Integral-Derivative (PID) controllers [7], [25] for their sway-yaw, pitch-heave, and surge velocity controllers. This greatly simplifies the control algorithms required to maintain and depth. More advanced methods which are often refinements of the classical PID controller can be used [25] to allow for closer track.

2.3 AUV cost considerations and limitations

Undersea vehicles designs are highly optimized for their mission set and their complexity results in high development coasts. Even in its simplest form, a UUV requires a robust control system, propulsion, actuation, sensors, power, and a structure

hardened against the ocean depth [14]. Every actuator or sensor requires some form of hardened hull penetration to prevent water intrusion from shorting out the interior electronics in addition to the system complexity. The complexity can quickly increase maintenance time and cost as additional actuation is required. The single bladed propeller, as depicted in Figure 2-3, can reduce the system complexity by using one actuator capable of providing 6 DOF actuation.



Figure 2-3: Example of a single bladed propeller

2.4 Prior work on single bladed propellers

Prior research into the single bladed propeller has focused on its feasibility as an actuation method [4], [12] efficiency in thrust production [4], and maneuvering control [10]. The single bladed propeller has proven to be a suitable method for AUV propulsion [4], [10], [12]. The single bladed propeller develops similar thrust to a conventionally multibladed propeller with higher efficiency at producing thrust in the forward thrust direction [4]. The single bladed propeller also provides an ability for the AUV to change course or depth by modulating the propeller's angular velocity resulting in an asymmetrical rotation [10], [12]. The asymmetrical rotation results in

difference in thrust provided by the AUV on one side of the AUV resulting in a net pitch or yaw moment as depicted in Figure 2-4. Kaeli, Littlefield, and Jaffre describe a calculation methodology for modeling the asymmetric thrust produced by the one blade propeller [10], [12] which can be incorporated into existing control theory and design simulation.

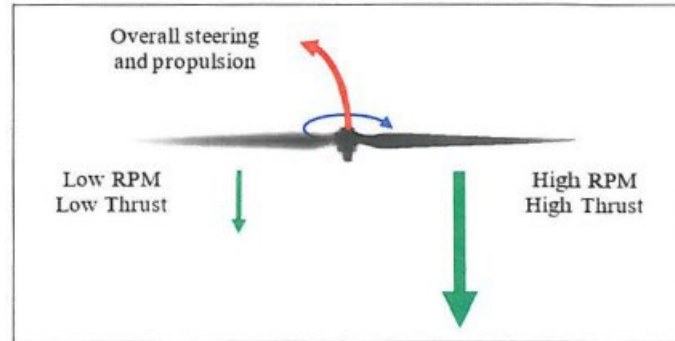


Figure 2-4: Example of single bladed propeller moment generation [4]

2.5 Single bladed propeller benefit

The greatest benefit of the single bladed propeller is its relative mechanical simplicity compared to other control actuation methods reducing cost. The single bladed propeller a single motor and propeller blade rather than the myriad of thrusters and fins required for actuation in 6 DOF for conventional AUVs. This reduces the mechanical complexity of the system.

2.6 Control system architecture

This thesis extensively uses Proportional-Integral-Derivative (PID) control for modeling AUV performance. PID control is a classical method for AUV closed loop feedback control systems [25] and many proposed control methods use modifications or linearization to enhance PID control [5], [21], [25]. A nominal closed loop feedback

control system is depicted in Figure 2-5. Equation 2.1 uses the error between the measured output and a reference value to change the model input to drive the error value to zero. PID control is commonly used due to its simplicity and ease of implementation. Equation 2.1 is the classical form of a PID controller transfer function.

$$D(s) = k_p + \frac{k_I}{s} + k_D s \quad (2.1)$$

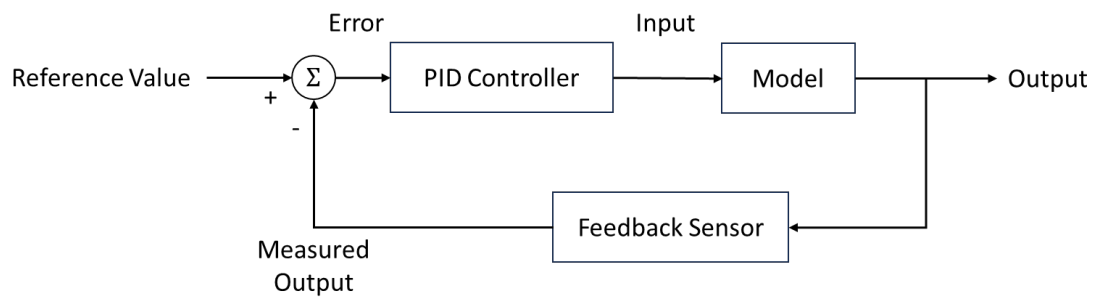


Figure 2-5: Closed loop feedback loop [25]

Instituting a PID controller requires tuning of the scalar gain values k_p , k_D , and k_I to ensure adequate performance. Generally, the k_p term is a scaling factor which provides a proportional ramp in motor or actuator output. The k_I term removes any steady-state error. The k_D term adds stability to the controller. $D(s)$ is a generic term for the error in a controlled parameter [25].

2.7 Applications and summary

A single bladed propeller will not be able to replace an ROV or an AUV in their specialized missions but it can provide enough capability to accomplish the design requirements for most applications. However, the simplicity of the single bladed propeller allows for it to be quickly built and quickly maintained. The reduced

production and maintenance time from the simpler system can result in AUV technology being available for a wider range of AUV users.

CHAPTER 3

DESIGN CASE STUDY

3.1 Introduction

This section details the development of the vehicle's hydrodynamic model, performance tests, and data analysis methods when applied to the Short Hulled AUV depicted in Figure 3-1. The design methodology described in section 1.2 was applied to the Short Hulled AUV to model its performance and assess the capability of the single bladed propeller. The key design parameter is the propeller blade length. The design characteristics of the Short Hulled AUV and its single bladed propeller are listed in Table 3-1 and depicted visually in Figure 3-2. Table 3-2 delineates the modeling assumptions used during the analysis.



Figure 3-1: Short Hulled AUV

Short Hulled AUV Key Design Characteristics		
Parameter	Variable	Value
Propeller Blade Length	l_p	0.0423 m
Max Propeller RPM	ω_{max}	3000 RPM
Min Propeller RPM	ω_{min}	250 RPM
Body Length	L	0.775 m
Body Radius	R	0.0672 m
Shroud Length	l_s	0.0511 m
Shroud Radius	r_s	0.0672 m
Main Cylinder Length	l_c	0.495 m
Nose Length	l_n	0.0445 m
Nose Radius	r_n	0.0223 m
Tail Cone Length	l_t	0.229 m
Tail Cone End Radius	r_t	0.0231 m
Sea Water Density	ρ_w	1025 kg/m ³
Propeller Angle of Attack	α_p	10.0 deg
Design Speed (goal)	U_d	1.50 m/s
Maximum Speed (goal)	U_{max}	2.50 m/s

Note: Bolded Parameters will be varied during analysis

Table 3-1: Short-Hulled AUV design characteristics

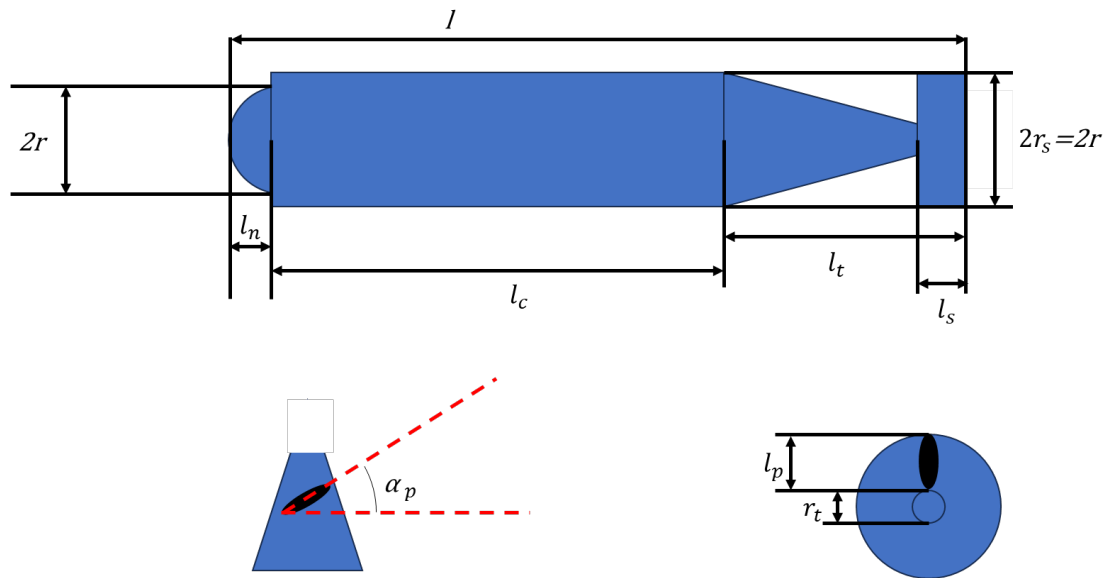


Figure 3-2: Short Hulled AUV measurement diagram

Modeling and Simulation Assumption	
Assumption	Justification
Neutrally Buoyant	AUV can be trimmed for neutral buoyancy. Simplifies analysis of depth changing performance.
Origin at Center of Gravity	Simplifies modeling of ships maneuvering dynamics. Center of Gravity can be designed to specific location within AUV.
Neglect depth related buoyancy changes	Minimal effect over range of depth change. Model intended for ideal maneuvering capability analysis.
Shroud effect on thrust is negligible	Isolates the performance of the one bladed propeller. Specific effects of shroud on propulsion capability unknown.
Hydrodynamic effects of small protuberances is negligible (i.e. knob, screw heads)	Minimal added mass from the screw heads, knob etc. Reduces complexity of the model. AUV does not operate at high enough speed for the effects of the protuberances to affect dynamics.
Stationary Fluid	Current effects are not necessary for this level of analysis.
Friction effects are due to skin friction only	AUV operates submerged minimizing the effects of residual drag forces.
Mass is uniformly distributed within AUV body	Mass distribution within the AUV is a design point. Minimal effect on the ideal vehicle dynamics.

Table 3-2: Modeling and simulation assumptions

3.2 Simulation and modeling approach

3.2.1 Coordinate system

The model in the succeeding sections uses a vehicle body-fixed coordinate system. The origin is located at the vehicle center of gravity as shown in Figure 3-3 and Figure 3-5. This coordinate system results in 6 directions of motion or DOF for the vehicle. The directions are surge (u), sway (v), heave (w), roll (p), yaw (q), and

pitch (r). X corresponds with the sum of external forces acting in the surge direction, Y corresponds with the sum of external forces acting in the sway direction, and Z corresponds with the sum of external forces acting in the heave direction. K corresponds with the sum of external moments acting in the roll direction, M corresponds with the sum of external moments acting in the pitch direction, and N corresponds with the sum of external moments acting in the yaw direction.

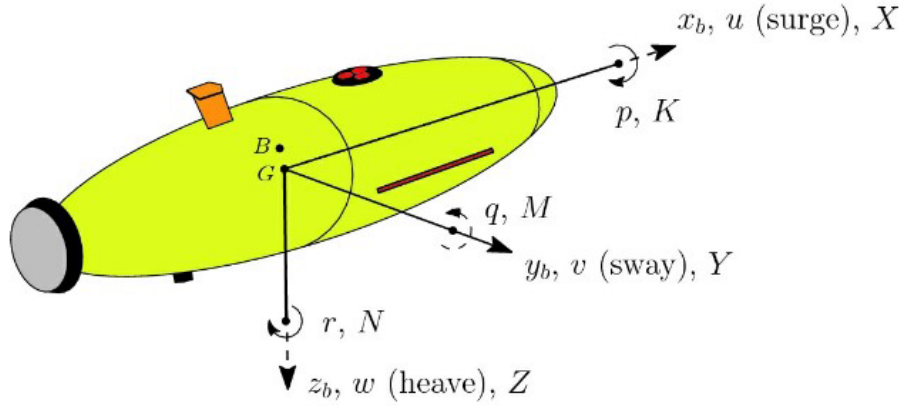


Figure 3-3: Body fixed coordinate system [25]

3.2.2 Rigid body equations of motion

The standard equations of motion for the six degrees of freedom described in equations 3.1 through 3.6 for the Body fixed coordinate system where m is the unit mass for the vehicle. (x_g, y_g, z_g) forms the components for the vector between the origin and the center of gravity.

$$m[\dot{u} - vr + wq - x_g(q^2 + r^2) + y_g(pq - \dot{r}) + z_g(pr + \dot{q})] = X \quad (3.1)$$

$$m[\dot{v} - wp + ur - y_g(r^2 + p^2) + z_g(qr - \dot{p}) + x_g(qp + \dot{r})] = Y \quad (3.2)$$

$$m[\dot{w} - uq + vp - z_g(p^2 + q^2) + x_g(rp - \dot{q}) + y_g(rq + \dot{p})] = Z \quad (3.3)$$

$$I_{xx}\dot{p} + (I_{zz} - I_{yy})qr - (\dot{r} + pq)I_{xz} + (r^2 - q^2)I_{yz} + (pr - \dot{q})I_{xy} + m[y_g(\dot{w} - uq + vp) - z_g(\dot{v} - wp + ur)] = K \quad (3.4)$$

$$I_{yy}\dot{q} + (I_{xx} - I_{zz})rp - (\dot{p} + qr)I_{xy} + (p^2 - r^2)I_{xz} + (qp - \dot{r})I_{yz} + m[z_g(\dot{u} - vr + wq) - x_g(\dot{w} - uq + vp)] = M \quad (3.5)$$

$$I_{zz}\dot{r} + (I_{yy} - I_{xx})pq - (\dot{q} + rp)I_{yz} + (q^2 - p^2)I_{xy} + (rq - \dot{p})I_{xz} + m[x_g(\dot{v} - wp + ur) - y_g(\dot{u} - vr + wq)] = N \quad (3.6)$$

Equations 3.8 through 3.13 show a simplification of the equations of motion accounting for the origin at the center of gravity using the simplification assumptions detailed in Table 3.2. In addition, the inertial tensor can be assumed to a diagonal matrix as described in Equation 3.7 due to port/starboard and bottom/top symmetry about the center of gravity.

$$\mathbf{I}_O = \begin{bmatrix} I_{xx} & 0 & 0 \\ 0 & I_{yy} & 0 \\ 0 & 0 & I_{zz} \end{bmatrix} \quad (3.7)$$

$$m[\dot{u} - vr + wq] = X \quad (3.8)$$

$$m[\dot{v} - wp + ur] = Y \quad (3.9)$$

$$m[\dot{w} - uq + vp] = Z \quad (3.10)$$

$$I_{xx}\dot{p} + (I_{zz} - I_{yy})qr = K \quad (3.11)$$

$$I_{yy}\dot{q} + (I_{xx} - I_{zz})rp = M \quad (3.12)$$

$$I_{zz}\dot{r} + (I_{yy} - I_{xx})pq = N \quad (3.13)$$

Factors of the sum of each external force or moment, X, Y, Z, K, M, and N may have a subscript corresponding to the effect on AUV dynamics due to an external force acting on the AUV body in a particular direction. For example, X_u is a coefficient indicating the external surge force acting on the AUV in the surge direction.

3.2.3 Hydrodynamic coefficient development

The external forces acting on the AUV due to the water flowing on the hull are quantified by developing a series of Hydrodynamic Coefficients. Two methods are commonly used to develop the Hydrodynamic Coefficients for an AUV, the prolate spheroid approximation and strip theory. The prolate spheroid approximation was chosen as the ultimate method for determining the added mass and hydrodynamic coefficients for the UUV. The prolate spheroid approximation greatly simplifies the generation of the added mass coefficients and can be reused for minor changes in the profile of the test vehicle. It can be quickly updated for follow on analysis while providing a representative model of the UUVs performance. Both the prolate spheroid approximation and the strip theory added mass and hydrodynamic coefficient methods are discussed in the following discussion for context.

3.2.3.1 Hull profile calculation

A typical UUV shape can be modeled by using a Myring hull profile where the hull geometry is defined as described in Chapter 8 of Fossen [7]. Equation 3.14 lays out the equations for characterizing a Myring hull profile. D is the diameter of the main hull cylinder, $r(x)$ is the radius of the hull at a given point on the hull, x is the distance from the beginning of the nose of the UUV to the point of interest. L_n is the point relative to the beginning of the nose to where the vehicle nose ends and the cylinder begins. L_c is the distance between the end of the hull cylinder and the beginning of the nose. L is the overall length of the entire vehicle.

$$r(x) \begin{cases} \left(\left(\frac{D}{2} \right)^2 - \left(\frac{D}{2} - x \right)^2 \right)^{1/2}, & 0 \leq x \leq L_n \\ \frac{D}{2}, & L_n < x < L_n + L_c \\ -0.2434 * (x - 21.2'') + D/2, & L_n + L_c \leq x \leq L \end{cases} \quad (3.14)$$

This method provides a standardized method for calculating and plotting the hull shape of a given UUV. The short hulled UUV in figure 3-1 follows a similar form factor. However, it uses a simplified hemispherical nose and a cone for the tail. These hull profile simplifications are shown in equation 3.14. The hull profile defined by equation 3.14 is used to calculate the added mass values associated with the short hulled UUV through strip theory. This method also provides the volume of the UUV hull for generating the prolate spheroid approximation added mass values. The UUV is assumed to be neutrally buoyant which allows for mass of the UUV to be calculated by mass of the water displaced by the UUV. The mass of the UUV is then used to solve for the dimensions of the prolate spheroid approximation.

This is possible due to the Myring hull profile being geometrically similar to a prolate spheroid and has been used before in [7] and [11] for added mass calculation.

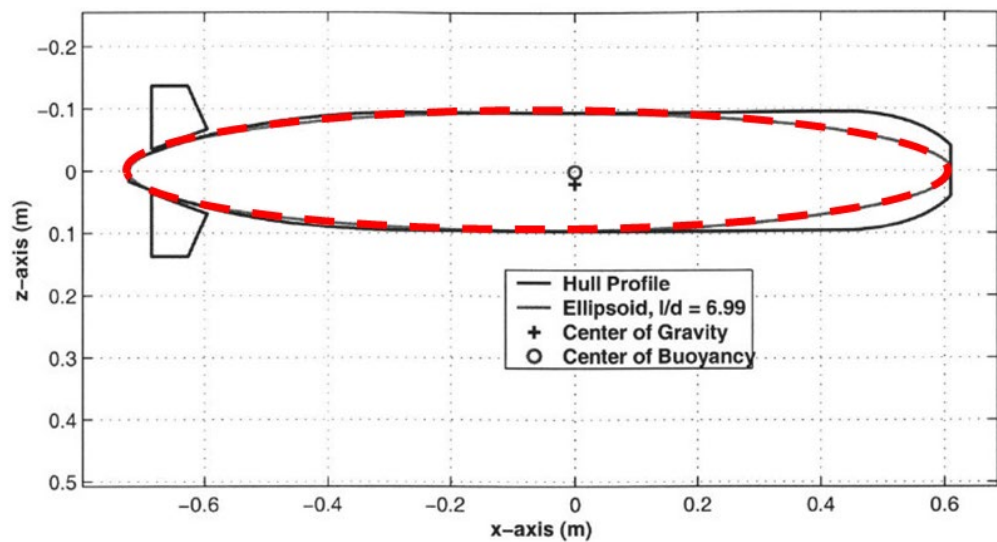


Figure 3-4: Prolate spheroid overlaid over a myring hull profile [19]

Figure 3-4 shows a prolate spheroid hull shape overlaid on a Myring hull profile to show the similarity. The axial length of the spheroid, $2a$ is set equal to the

overall length of the vehicle length. This allows for calculating the radius of the prolate spheroid using equation 3.15. Where m is the vehicle mass, ρ_w is the water density, a half of the overall length of the vehicle, and b is the radius of the prolate spheroid at the midpoint.

$$m = \frac{4}{3}\pi\rho_w ab^2 \quad (3.15)$$

A set of cruciform 3” by 3” tail fins are added to both the prolate spheroid and actual test shape model 24.2” down the length of the hull from the nose to allow for the comparison of the rudder performance to single bladed propeller performance. This mock up is displayed by Figure 3-5 on both the prolate spheroid and generic AUV shape. The rudder and fin configuration is only used to determine performance of a conventionally actuated AUV for comparison to the single bladed propeller model. It is removed for the singled bladed propeller tests. Both the rudder actuated and propeller actuated models incorporate the hydrodynamic contribution of the shroud. The shroud was too large to have negligible effect on the cross flow drag acting on the AUV.

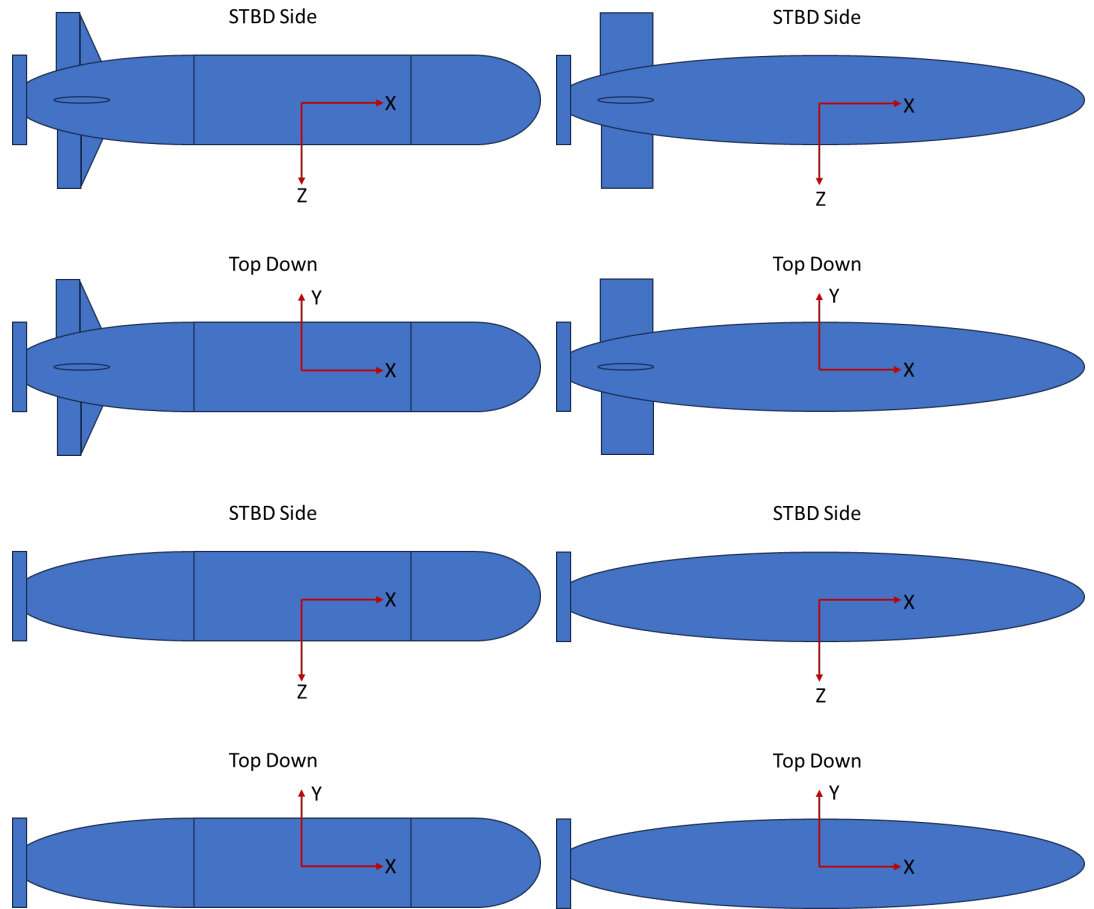


Figure 3-5: Conventional test shape (upper left), conventional prolate spheroid (upper right), single bladed test shape (lower left), and single bladed prolate spheroid (lower right).

3.2.3.2 Strip theory

The UUV was modeled for course and depth control using a linearized dynamic model for small perturbations. The rigid body mass is tabulated in the matrix form given in equation 3.16 which includes an assumption for Top/Bottom and Port/Starboard symmetry following [4] and [7]. The added mass forces and moments are tabulated in matrix form given in equation 3.17. Direction 1 in the mass matrix corresponds with the surge (u) direction, 2 with sway (v), 3 with heave (w), 4 with roll (p), 5 with pitch (q), and 6 with yaw (r).

$$m_{RB} = \begin{bmatrix} m & 0 & 0 & 0 & 0 & 0 \\ 0 & m & 0 & 0 & 0 & 0 \\ 0 & 0 & m & 0 & 0 & 0 \\ 0 & 0 & 0 & I_x & 0 & 0 \\ 0 & 0 & 0 & 0 & I_y & 0 \\ 0 & 0 & 0 & 0 & 0 & I_z \end{bmatrix} \quad (3.16)$$

$$m_A = \begin{bmatrix} m_{11} & 0 & 0 & 0 & 0 & 0 \\ 0 & m_{22} & 0 & 0 & 0 & m_{26} \\ 0 & 0 & m_{33} & 0 & m_{35} & 0 \\ 0 & 0 & 0 & m_{44} & 0 & 0 \\ 0 & 0 & m_{53} & 0 & m_{55} & 0 \\ 0 & m_{62} & 0 & 0 & 0 & m_{66} \end{bmatrix} \quad (3.17)$$

The added mass and drag force coefficients were calculated using two methods. The first method used strip theory approximations from slender body theory [11], [19]. Equation 3.18 was used for circular cross sections while equation 3.19 incorporated the contributions from the fins. Where a_{fin} is the height of the fin/rudder above centerline, $R(x)$ is the hull radius at a given point of x , and ρ_w is the water density.

$$m_a(x) = \pi\rho_w R(x)^2 \quad (3.18)$$

$$m_{af}(x) = \pi\rho_w \left(R(x)^2 + \frac{(a_{fin}^2 - R(x)^2)^2}{a_{fin}^2} \right) \quad (3.19)$$

Equations 3.20 through 3.25 were used to calculate added mass. These derivations were used in [19] for developing the hydrodynamic coefficients of a REMUS 100 vehicle. The viscous drag forces were calculated using equations 3.26-3.29. This process was conducted for both the conventionally actuated and the single bladed propeller actuated UUV. The viscous and drag force equations were useful for calculating hydrodynamic contribution of the fins and propeller shroud as applicable.

$$m_{22} = m_{33} = \int_{x_c}^{x_{finstart}} m_a(x)dx + \int_{x_{finstart}}^{x_{finend}} m_{af}(x)dx + \int_{x_{finstart}}^{x_{tail}} m_a(x)dx \quad (3.20)$$

$$Y_{\dot{v}} = Z_{\dot{w}} = -m_{22} = -m_{33} \quad (3.21)$$

$$m_{62} = m_{53} = - \int_{x_c}^{x_{finstart}} x m_a(x)dx + \int_{x_{finstart}}^{x_{finend}} x m_{af}(x)dx + \int_{x_{finend}}^{x_{tail}} x m_a(x)dx \quad (3.22)$$

$$N_{\dot{v}} = Y_{\dot{r}} = -M_{\dot{w}} = -Z_{\dot{q}} = -m_{62} = -m_{26} = m_{53} = m_{35} \quad (3.23)$$

$$m_{66} = m_{55} = \int_{x_c}^{x_{finstart}} x^2 m_a(x)dx + \int_{x_{finstart}}^{x_{finend}} x^2 m_{af}(x)dx + \int_{x_{finstart}}^{x_{tail}} x^2 m_a(x)dx \quad (3.24)$$

$$N_{\dot{r}} = M_{\dot{q}} = -m_{55} = -m_{66} \quad (3.25)$$

$$Y_v = Z_w = -\frac{1}{2}\rho_w c_{dc} \int_{x_c}^{x_t} 2R(x)dx - 2 * \left(\frac{1}{2}\rho_w c_{df} A_{fin}\right) \quad (3.26)$$

$$M_w = -N_v = \frac{1}{2}\rho_w c_{dc} \int_{x_c}^{x_t} 2xR(x)dx - 2x_{fin} * \left(\frac{1}{2}\rho_w c_{df} A_{fin}\right) \quad (3.27)$$

$$Y_r = -Z_q = -\frac{1}{2}\rho_w c_{dc} \int_{x_c}^{x_t} 2x|x|R(x)dx - 2x_{fin}|x_{fin}| * \left(\frac{1}{2}\rho_w c_{df} A_{fin}\right) \quad (3.28)$$

$$N_r = M_q = -\frac{1}{2}\rho_w c_{dc} \int_{x_c}^{x_t} 2x^3 R(x)dx - 2x_{fin}^3 * \left(\frac{1}{2}\rho_w c_{df} A_{fin}\right) \quad (3.29)$$

3.2.3.3 Prolate spheroid approximation

The prolate spheroid approximation used equations 3.30-3.36 to calculate the added mass coefficients. These include the moment of inertia for the prolate spheroid model. The strip theory moments of inertia were calculated using traditional parallel axis theory and area calculations. The value, e , is the eccentricity of the prolate spheroid and is used to calculate the constants α_0 and β_0 .

$$e = 1 - \left(\frac{b}{a}\right)^2 \quad (3.30)$$

$$\alpha_0 = \frac{2(1-e^2)}{e^3} \left(\frac{1}{2} \ln \frac{1+e}{1-e} - e \right) \quad (3.31)$$

$$\beta_0 = \frac{1}{e^2} - \frac{1-e^2}{2e^3} \left(\ln \frac{1+e}{1-e} \right) \quad (3.32)$$

$$m_{11} = -\frac{\alpha_0}{2-\alpha_0} m \quad (3.33)$$

$$m_{22} = m_{33} = -\frac{\beta_0}{2-\beta_0} m \quad (3.34)$$

$$m_{44} = K_{\dot{p}} = 0 \quad (3.35)$$

$$m_{66} = m_{55} = -\frac{1}{5} \frac{\left((b^2 - a^2)^2 (\alpha_0 - \beta_0) \right)}{2(b^2 - a^2) + (b^2 + a^2)(\beta_0 - \alpha_0)} \quad (3.36)$$

The fins were approximated as flat plate using the calculated using equations 3.37-3.41 [11]. Figure 3-6 shows the dimensions used for a pair of identically sized control fins. This process was repeated for the single bladed propeller with the control fins removed. This is expected as added mass is known to be off by as much as 100% [11], [19].

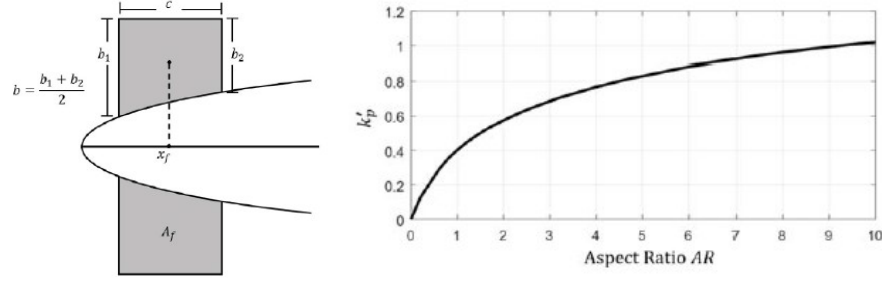


Figure 3-6: Dimensions for a pair of identically sized control fins (left), Coefficient of additional moment of inertia for a flat plate (right) [11]

$$Y_{\dot{v}_f} = -2 \left(\frac{k_p \rho_w c^2 b}{4} \right) \quad (3.37)$$

$$Y_{\dot{r}_f} = Y_{\dot{v}_f} x_f \quad (3.38)$$

$$N_{\dot{r}_f} = -2 \left(\frac{1}{48} k'_p \rho_w c^3 b^2 \right) + Y_{\dot{v}_f} x_f^2 \quad (3.39)$$

$$k_p = \frac{1}{\sqrt{1 + \frac{1}{AR}}} \quad (3.40)$$

$$AR = \frac{b^2}{A_{fin}} \quad (3.41)$$

3.2.3.4 Control surface force coefficient calculation

The lift on the fins was calculated using equations 3.42 and 3.43. These were taken from Prestero [19]. Where c_L is the coefficient of lift, A_{fin} is the planform area of the fin, α is the angle of attack of the fin, ρ_w is the water density, and U is the surge velocity of the UUV. The axial location of the fin, x_f , was taken relative to the center of gravity of the UUV.

$$Z_{w\delta fin} = Y_{v\delta fin} = \frac{1}{2} \rho_w c_L A_{fin} \alpha U^2 \quad (3.42)$$

$$N_{v\delta fin} = M_{w\delta fin} = x_f Z_{w\delta fin} = x_f Y_{v\delta fin} \quad (3.43)$$

The fin lift coefficient was found using equation 3.44, the Hoerner approximation from [11] for high AR foils. $\bar{\alpha}$ was assumed to be 0.9 as described in by Carelli [4].

The AR of the fins was calculated using the equation 3.41. Since the fins were attached to the body, there is only one side which experiences vortex shedding which allows effective AR of the fins to be doubled. The moment calculated in equation 3.43 uses the axial location of the fins x_f to calculate the moment produced by the fins. This follows the traditional methods for fin control laid out by [7], [11], and [19].

$$c_{L\alpha} = \frac{dc_L}{d\alpha} = \left(\frac{1}{2\bar{\alpha}\pi} + \frac{1}{\pi AR} + \frac{1}{2\pi(AR)^2} \right)^{-1} \quad (3.44)$$

The single bladed propeller modeling is derived in [10] and [12]. The blade velocity is modulated throughout its angular rotation. The angular velocity, ω , is varied as a function of angular position with peak ω , ω_2 , on one side of the UUV and the minimum ω , ω_1 , is on the opposite side of the UUV. The average force is calculated using equation 3.45. Where c_f is the thrust coefficient for the propeller, α is the propeller angle of attack, R_{prop} is the span length of the propeller, ω_1 is the minimum propeller angular velocity and ω_2 is the maximum propeller angular velocity.

$$F_{prop} = \frac{c_F \rho a}{16} R_{prop}^4 (\omega_1^2 + \omega_2^2) \quad (3.45)$$

The moment is calculated by multiplying the propeller force by the moment arm $r \cos(\theta - \phi)$ where ϕ is the steering angle or the orientation of the maximum moment and θ is the current orientation of the propeller. Figure 3-7 depicts an example of the relationship between the steering angle and the propeller orientation. However, by taking the average moment this results in equation 3.46 as derived in [10] and [12].

$$M_{prop} = -\frac{c_F \rho a}{10\pi} R_{prop}^5 (\omega_2^2 - \omega_1^2) \sin(\phi) \quad (3.46)$$

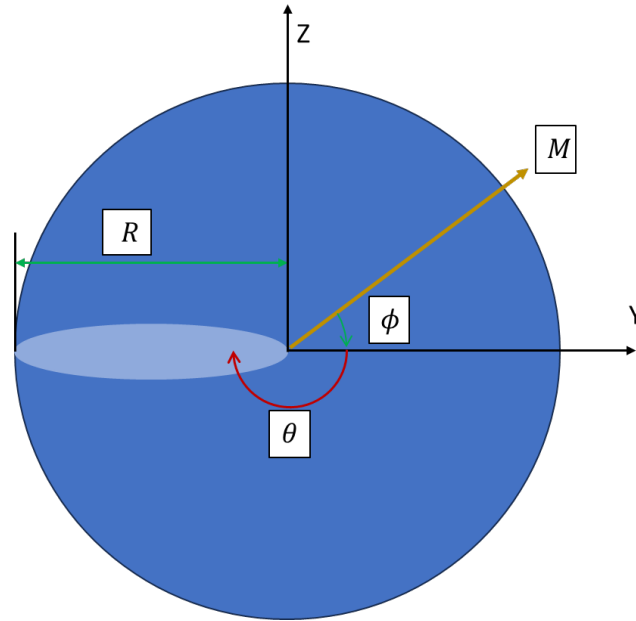


Figure 3-7: Steering angle and propeller orientation relationship

The difference in ω_2 and ω_1 results in a maximum turning moment applied in the direction of the steering angle. The steering angle can be calculated equation 3.47 where e and r are the normalized lift and course demand. The lift and course demand are normalized to where $e=r=1$ corresponds with the maximum yaw or pitch moment. For simplicity, the vehicle was modeled with depth and course control decoupled which makes the $\sin(\phi)$ always equal to -1 or 1 corresponding to the direction of the desired course or pitch angle change. Figure 3-8 depicts an example of the steering angle applied to correct a course perturbation while assuming constant depth.

$$\phi = \tan^{-1} \left(\frac{e}{r} \right) \quad (3.47)$$

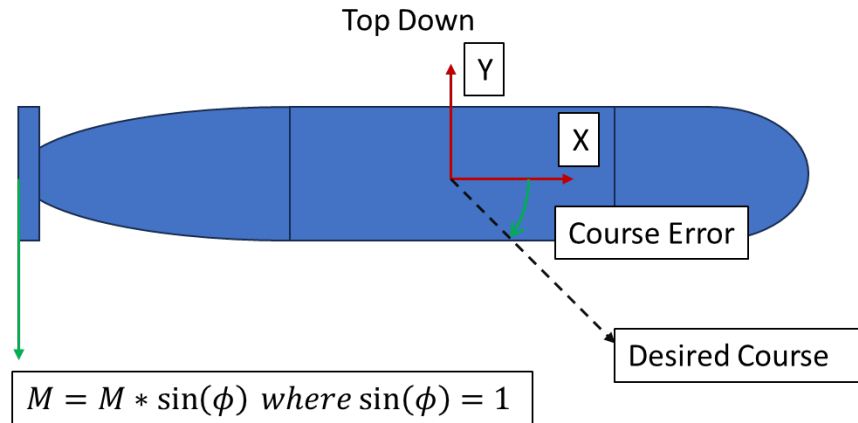


Figure 3-8: Steering angle applied to a decoupled course controller.

3.2.4 Model linearization

A linear state space model was used for the rigid body dynamics of the system. Three separate linear state space models were developed. One for sway-yaw control (course), one for pitch-heave control (depth), and another for surge velocity control (speed). These three models were then combined into one Coupled Dynamic Controller model.

3.2.4.1 Linearized time invariant system

The performance models were developed as Linearized Time Invariant (LTI) system. The key point with this style of system is to model vehicles around a desired operating point. Control is used to keep the system at the operating point to linearize the system and simplify models and calculations. An LTI system applies to this model as none of the equations of motion for the simulations are considered time varying. Instead, they are a factor of position, force, and moments. The LTI property of the modeling systems allow for a state space model to be applied. This proved to be very useful as it allowed for similar control and modeling algorithms to be applied to each specific model. The generic state space model is described by equations 3.48 and 3.49.

$$\dot{x}(t) = \mathbf{A}x(t) + \mathbf{B}u(t) \quad (3.48)$$

$$y = \mathbf{C}x(t) + \mathbf{D}u(t) \quad (3.49)$$

In the state space models above \dot{x} , x , y , and u are vectors. A , B , C , and D are considered matrices with coefficients corresponding with AUV dynamics. The state vector comprises of x and \dot{x} which completely describes the system state. The output vector, y , provides the measurement of the state for control feedback. The input vector, u , provides the effect of the control inputs.

Equation 3.50 describes the general form of a dynamic system model developed using the hydrodynamic coefficient approach described above. The following equations describe the process to derive the A , and B matrices. The C matrix consists of an identity matrix defined by the states of interest for the given system. Essentially, each “1” in the identity matrix corresponds with a state variable of interest. The D matrix is 0 in practice. The M , N , and b matrices are populated using the hydrodynamic coefficient estimates described above.

$$\mathbf{M}\dot{x} + \mathbf{N}x = \mathbf{b}u \quad (3.50)$$

$$\dot{x} = -\mathbf{M}^{-1}\mathbf{N}x + \mathbf{M}^{-1}\mathbf{b}u \quad (3.51)$$

$$\mathbf{A} = -\mathbf{M}^{-1}\mathbf{N}x \quad (3.52)$$

$$\mathbf{B} = \mathbf{M}^{-1}\mathbf{b}u \quad (3.53)$$

3.2.4.2 Sway-yaw model

Equations 3.56, 3.57, and 3.58 are the matrices for the LTI system described in the previous section applied for Sway-Yaw dynamics. These equations are generated from the non-linear 6- DOF Rigid Body Equations of Motion discussed above. By assuming motion occurs only in the XY plane where the AUV has planar symmetry in

the XZ plane a 3 DOF linearized 3-DOF model can be developed for Sway-Yaw control by removing the pitch, roll, and depth terms. Then by neglecting memory effects and eliminating nonlinear terms, equations 3.54-3.55 can be developed.

Equation in the M, N, and b matrix form result in equations 3.56-3.58.

$$(m - Y_{\dot{v}})\dot{v} - Y_v v + (mx_g - Y_{\dot{r}})\dot{r} + (mU - Y_r)r = Y_{control} \quad (3.54)$$

$$(I_{zz} - Y_{\dot{r}})\dot{r} + (mx_g U - N_r)r + (mx_g - N_{\dot{v}})\dot{v} - N_v v = N_{control} \quad (3.55)$$

$$M = \begin{bmatrix} m - Y_{\dot{v}} & mx_g - Y_{\dot{r}} & 0 \\ mx_g - N_{\dot{v}} & I_{zz} - N_{\dot{r}} & 0 \end{bmatrix} \quad (3.56)$$

$$N = \begin{bmatrix} -Y_v & mU - Y_r & 0 \\ -N_v & mx_g U - N_r & 0 \\ 0 & -1 & 0 \end{bmatrix} \quad (3.57)$$

$$b = \begin{bmatrix} 0 \\ N_{prop} \\ 0 \end{bmatrix} \quad (3.58)$$

In this case, course control is accomplished using PID control. The PID controller uses the course error as the input and generates an unitless output from 0 to 1 which represents the “rudder” demand of the one bladed propeller. The rudder demand is used to generate the desired propeller angular velocity difference to generate the moment to turn the AUV. Table 3-3 includes the PID controller coefficient values for the sway yaw controller. The K_I value is set for 0.000 after modeling and simulation revealed the additional integral term did not provide significant performance improvement. Equation 3.46 describes the equation defining the moment generated by the propeller angular velocity difference.

Sway-Yaw PID Controller Coefficients	
K_P	30.0
K_I	0.00
K_D	40.0

Table 3-3: Sway yaw PID controller coefficients

3.2.4.3 Pitch-heave model

Equations 3.59, 3.60, and 3.61 are the matrices for the LTI system described in the previous section applied for Pitch-Heave dynamics. The inner controller controls the pitch angle taking the pitch angle error as the input and generates an unitless output from 0 to 1 which represents the “elevator” demand of the one bladed propeller. The “elevator” demand is used to generate the desired propeller angular velocity difference to generate the moment to turn the AUV. Equation 3.46 describes the equation defining the moment generated by the propeller angular velocity difference. The outer controller uses depth error as the input to generate the desired pitch angle to generate heave velocity to change depth. The desired pitch angle is then applied to the inner controller. Table 3-4 depicts the PID coefficients for the pitch heave controller. The inner controller uses $K_I = 0.00$ since as the integral value provided minimal performance improvement in assessing the AUV performance.

$$M = \begin{bmatrix} m - Z_{\dot{w}} & -mx_g - Z_{\dot{q}} & 0 \\ -mx_g - M_{\dot{w}} & I_{yy} - M_{\dot{q}} & 0 \end{bmatrix} \quad (3.59)$$

$$N = \begin{bmatrix} -Z_w & -mU - Z_q & 0 \\ -M_w & mx_g U - M_q & 0 \\ 0 & -1 & 0 \end{bmatrix} \quad (3.60)$$

$$b = \begin{bmatrix} 0 \\ M_{prop} \\ 0 \end{bmatrix} \quad (3.61)$$

Pitch Heave PID Controller Coefficients	
K_P Pitch	1.50
K_I Pitch	0.00
K_D Pitch	100.0
K_P Depth	1.00
K_I Depth	0.00
K_D Depth	0.00

Table 3-4: Pitch heave PID controller coefficients

3.2.4.4 Surge velocity model

Equations 3.62, 3.63, and 3.64 are the matrices for the LTI system described in the previous section applied for Surge Velocity dynamics. Equation 3.65 calculates the drag force acting on the AUV. A PID controller was incorporated for the Surge Velocity controller. However, K_p was the only nonzero PID coefficient and $K_p = 1$. This provided sufficient performance and minimized complexity of the controller.

$$M = [m - X_{\dot{u}}] \quad (3.62)$$

$$N = [X_u] \quad (3.63)$$

$$b = [X_{prop}] \quad (3.64)$$

$$X_u = \rho_{sw} C_d A U \quad (3.65)$$

3.2.4.5 Coupled controller model

The coupled controller model incorporated the preceding models to model a combination course, depth, and speed change. The combination of the course and depth change models was relatively easy to institute since the model presented in [10] incorporated depth and course control functions and simply required applying equation 3.66 to calculate the steering angle given a compound course and depth perturbation. In the independent Sway-Yaw and Pitch-Depth models, the steering

angle had been hard coded as -1 or 1 based on the sign of the perturbation. However, the challenge became incorporating the surge velocity. For simplicity, the AUV was given an average propeller RPM (ω_{avg}) to maintain based on surge velocity vs. propeller RPM plots developed during the surge velocity performance tests. The maximum RPM, ω_2 , and minimum RPM, ω_1 , were allowed to vary based on equation 3.66 to provide a simple version of surge velocity control. At saturation $\omega_2 = \omega_{upper\ limit}$ and $\omega_1 = \omega_{min}$.

$$\omega_{upper\ limit} = (2 * \omega_{avg}^2 - \omega_{min}^2) \quad (3.66)$$

3.2.5 Single bladed propeller thrust and torque characterization

In conventional propeller performance modeling, c_f is described as K_T where K_T is the thrust coefficient for the propeller based on the advance ratio, J , of the ship. J is calculated using equation 3.67 where u_a is the advance speed of the propeller in the wake of the hull, n is the propeller angular velocity, and the D is the propeller diameter [7], [27]. J is a non-dimensional value from which K_T and K_Q , propeller torque coefficient, can be calculated using equations 3.68 and 3.69 where T is the thrust and Q is the propeller torque opposing propeller motion [7]. The efficiency of the propeller can be described by equation 3.70 using the previously discussed term [7]. For the purposes of this thesis, the AUV was assumed to be traveling through uniform flow and $u_a = U$ or the surge velocity of the AUV. It was determined from Carelli [4] that K_T is a design parameter for the propeller and the propeller will be somewhat constant during steady state operations. K_T changes primarily in large speed changing transients allowing for a constant $K_T = 0.14$ to be assumed for testing.

Carelli's open water propeller performance curve is depicted in Figure 3-9 indicating the expected K_T , K_Q , and open water efficiency.

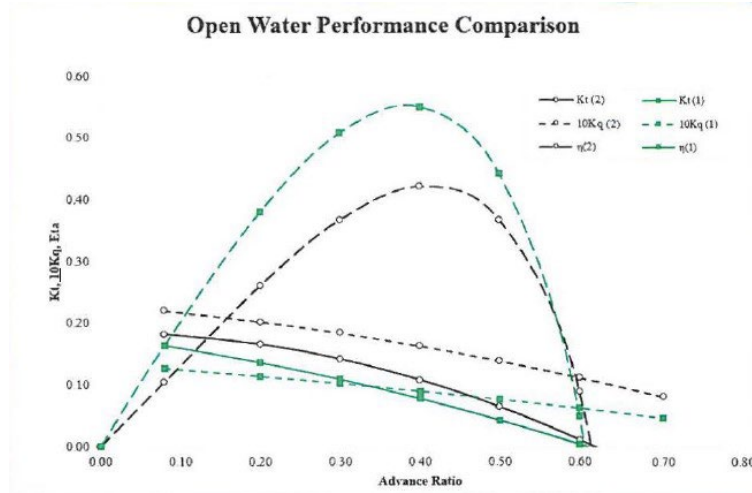


Figure 3-9: Carelli open water propeller performance curves [4]

$$J = \frac{u_a}{nD} \quad (3.67)$$

$$K_T = \frac{T}{\rho_w D^4 |n|} \quad (3.68)$$

$$K_Q = \frac{Q}{\rho_w D^5 |n|} \quad (3.69)$$

$$\eta = \frac{J K_T}{2\pi K_Q} \quad (3.70)$$

Figure 3-9 depicts the thrust coefficient associated with an unshrouded single bladed propeller which results in the modeling and simulation assuming there are no thrust effects associated with the shroud. Additional testing will be conducted applying the effects of the propeller shroud.

3.3 MATLAB/SIMULINK implementation

The model was encoded into Math Works MATLAB and SIMULINK version R2022b. MATLAB was used to generate the LTI State Space model discussed in 3.2.4.1 as well as the various constants and initial conditions associated with each test. SIMULINK was used to conduct simulations of the AUV maneuvers. The SIMULINK model included the separate control schemes for each of the sway-yaw, pitch-heave, and surge velocity subsystems. Both the course and surge velocity controllers used generic PID controller architecture described in section 2.6 and in sections 3.2.4.2 and 3.2.4.4. The depth controller used nested PID controller architecture as discussed in section 3.2.4.3. Individual SIMULINK scripts were used for the initial tests uncoupled dynamic tests. A coupled controller was developed to combine the three subsystems into a single simulation model using the methods described in section 3.2.4.5. The simulation model would then generate simulation outputs retrievable by MATLAB. MATLAB was used to sift through the simulation output data to aid in analysis.

3.4 Applying the propeller sizing procedure

This section discusses the application of the propeller sizing procedure to the design of the “short hulled” AUV to assess the maneuvering capability of the single bladed propeller. AUV maneuvering performance was assessed using the model developed in the preceding sections. The modeled AUV design was then subjected to a number of Course, Depth, and Speed performance tests. The two primary variables for these tests were the propeller blade size and allowable RPM difference.

3.4.1 Determine propeller RPM as a function of blade length for design maximum speeds.

The model was given an initial speed to maintain using the surge velocity controller. The simulation initiated with the model at 90% of its desired surge velocity then it was allowed to attempt to attain that speed. 10% was selected to allow for the model to be maintained within its linearized operating point. The desired surge velocity was increased in 0.5 m/s increments until the propeller was determined to be saturated. The propeller RPM and actual surge velocity was recorded at each increment. Saturation was indicated when the model reached maximum propeller RPM and actual surge velocity did not increase. Then, the desired speed was decreased by 0.25 m/s to validate the saturation surge velocity. The actual surge velocity and propeller RPM were plotted to determine their relationship for use in the coupled controller plots. Figure 3-10 provides an example of the surge velocity vs. propeller RPM plot. A linear relationship is assessed between the surge velocity and the propeller RPM as shown in equations 3.71 – 3.74 provided the AUV is not changing course or depth and $\omega_1 = \omega_2$. An equation for the line of best fit between the steady state Surge Velocity and steady state Propeller RPM was generated and used in the maneuvering performance tests. This was used to determine the necessary baseline propeller RPM required to maintain the desired surge velocity through a maneuver.

$$F_{drag} = \frac{1}{2} C_d \rho_w A U^2 = F_{prop} = \frac{1}{16} C_F \rho_w \alpha (\omega_2^2 + \omega_1^2) \quad (3.71)$$

$$\omega_1 = \omega_2 \quad (3.72)$$

$$C_d A U^2 = \frac{1}{8} C_F \alpha \omega_2^2 \quad (3.73)$$

$$\sqrt{\frac{8C_dA}{C_F\alpha}} * U = \omega_2 \quad (3.74)$$

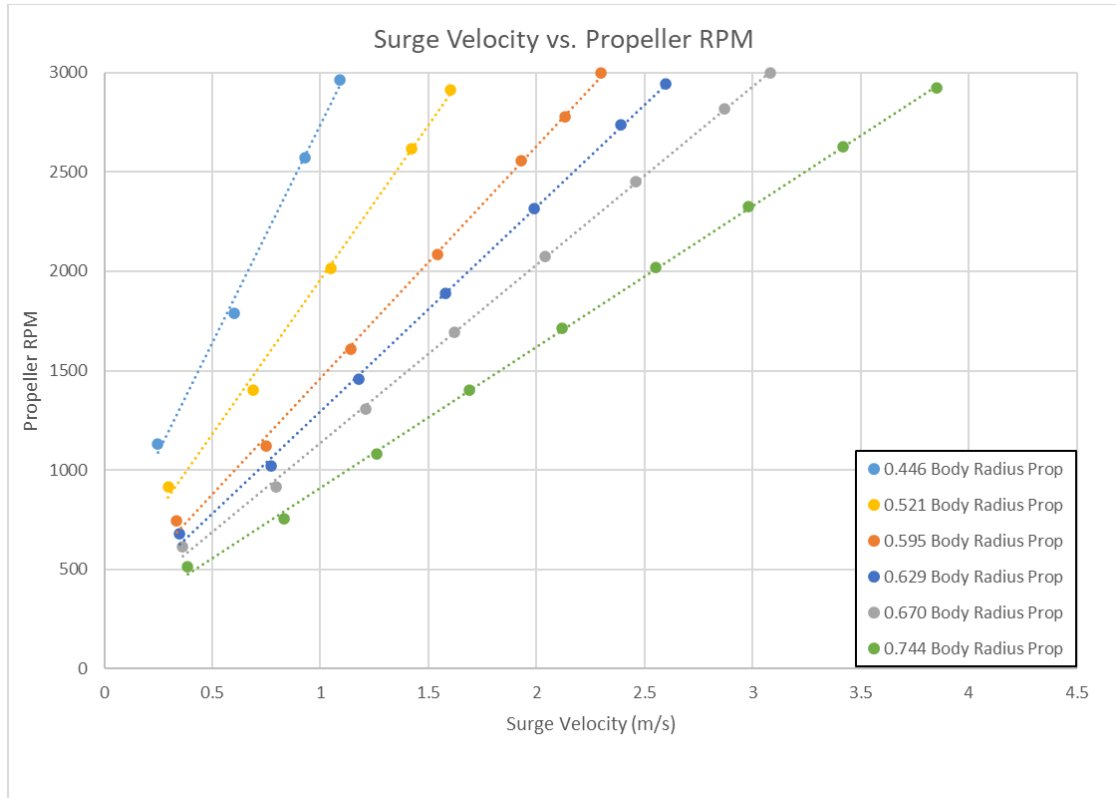


Figure 3-10: Surge velocity vs. propeller RPM example

The propeller blade size was tested by repeating the performance assessment tests using various sizes of the propeller blade as depicted in Figure 3-10. The surge velocity tests were found to be the best starting point for these tests. The AUV must be able to maintain its design surge velocity regardless of its required course and depth change. The propeller blade size range was varied between 0.446 body radius and 0.744 body radius to assess its viability. The “short hulled” AUV uses a propeller measuring 0.629 body radius and this propeller blade region provides sufficient variation in performance to assess the effects of the propeller blade size. The resulting

Surge Velocity vs. Propeller RPM plots were used to select a range of viable propeller blade lengths to be used for the course and depth performance tests. A second test was conducted using the “short hulled” AUV propeller blade size incorporating the effect of the shroud to assess the increase in performance.

3.4.2 Model advance, transfer, tactical diameter, and depth changing performance as a function of speed and propeller diameter

The course and depth changes were conducting with $\omega_1 = 250$ RPM and $\omega_2 = 3000$ RPM. 3000 RPM is the maximum permitted speed for the propeller blade assembly developed by Kaeli at Armada Robotics [2], [10]. 250 RPM was selected to prevent the propeller RPM from reaching zero in the simulation while providing ample RPM differential for results. This RPM differential would be varied in subsequent tests but the maximum permitted differential was used to model maximum turning capability of each propeller blade size. Equation 3.64 can be used with the minimum ω_1 and maximum ω_2 achieved to determine the average propeller RPM maintained through the turn. This value can then be used to determine ideal AUV surge velocity through the turn to provide maximum turning performance.

3.4.2.1 Course changing open loop test

The model was given a 180 degree course perturbation then allowed to correct to a 000 degree course. 180 degrees was selected because it provided the classical critical maneuvering characteristics of a sea vessel: advance, transfer, and tactical diameter in body lengths. An example of these parameters is included in Figure 3-11. In addition, the turn rate and maneuver time was collected. A control test was conducted with the same hull form using a rudder and retaining the same data.

Another test was conducted using the “short hulled” AUV propeller blade size incorporating the effect of the shroud to assess the increase in performance.

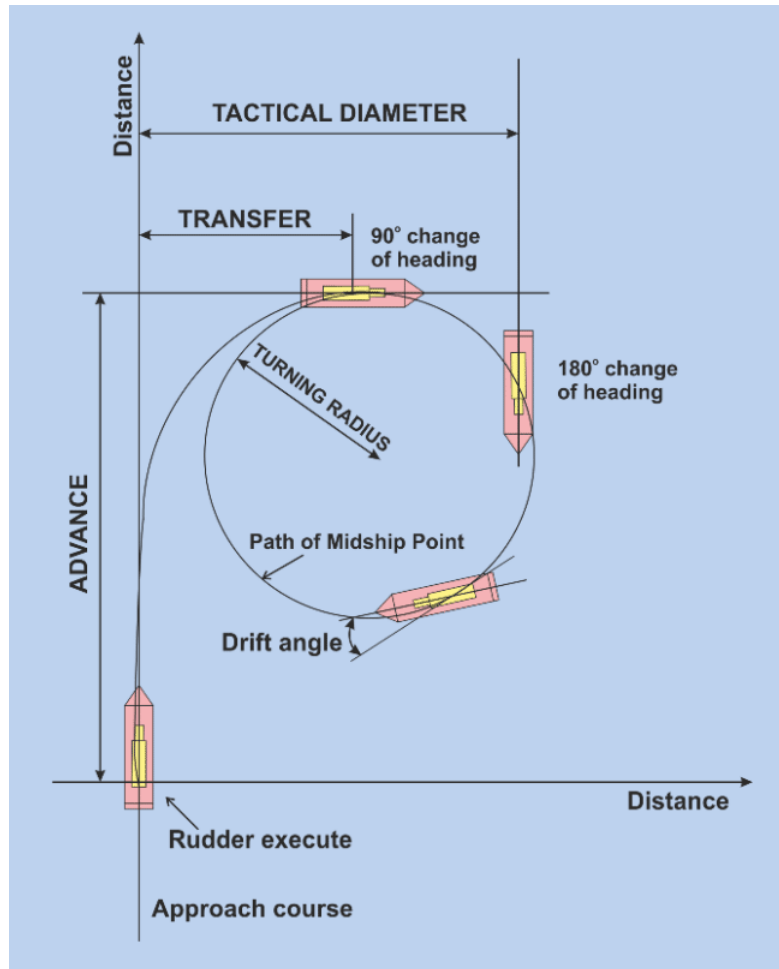


Figure 3-11: Maneuvering characteristics example [8]

3.4.2.2 Depth changing open loop test

The model was given a 10 m change and the depth overshoot, settling time, and depth rate were retained. A 10 m depth change was selected because it provided ample time for the AUV to initiate the maneuver, settle on its steady state pitch angle, and finish the maneuver when the desired depth was reached. A control test was conducted with the same hull form using control fins and retaining the same data.

3.4.2.3 Angular velocity differential tests

After the propeller blade length tests were completed another series of tests at each propeller blade size was conducted at varying allowed angular velocity difference (ω_{diff}) to determine the overall effect of ω_{diff} . These tests were first conducted with $\omega_{\text{diff}} = 2750$ RPM and then ω_{diff} was reduced in 250 RPM increments. Each test was repeated using the same performance tests as above to determine the effect of ω_{diff} on vehicle performance.

3.4.2.4 Composite control tests

There were two parts of the composite control tests. The first style of test incorporated speed control into a course or depth change. This was done by using the surge velocity vs. propeller RPM equations determined in section 3.4.1 to calculate the necessary average ω to maintain a given surge velocity through a maneuver. The control algorithm was updated using equation 3.66 to determine the maximum RPM, ω_2 , to ensure the average F_{prop} was the same as the F required to maintain constant surge velocity. The minimum RPM, ω_1 , was allowed to vary. $\omega_{\text{max}} = 3000$ RPM and $\omega_{\text{min}} = 250$ RPM for the simulation. The course and depth performance open loop tests were then repeated for 0.5 to 2.5 m/s.

The second form of the composite control tests combined the course and depth performance open loop tests. The model simulated a simultaneous 180 degree course change and 10 m depth change while attempting to maintain a constant surge velocity through the maneuver.

3.5 Data analysis

Table 3-5 lists the data retained for each test. The performance of the model was compared to the rudder actuated version. The data was then used to characterize the performance of the single bladed propeller. Post processing of the data results in an operating envelope showing the expected maximum and minimum propeller angular velocity at each test speed. This data can be used to assess regions of expected improved or reduced maneuvering performance based on the desired surge velocity of the AUV as depicted in Figure 3-12.

Figure 3-12 depicts the operating envelope of the AUV while surge velocity control is established. The upper line for each propeller blade size is the maximum propeller angular velocity, ω_2 , during the maneuver. The lower line for each propeller blade size is the minimum propeller angular velocity, ω_1 , observed during the maneuver. The region in between the two lines represents a region where the AUV control software can select the desired ω_{diff} through the maneuver. The widest portion between the curves indicates the “ideal” turning speed where the AUV can maintain its desired speed while maximizing turning performance. The region between the curve narrows as it needs to limit ω_{diff} to maintain the desired surge velocity. Once the upper curve flattens, the AUV propeller is considered saturated while trying to maintain its desired surge velocity and its turning performance degrades. The lower curve is flat where the AUV propeller needs $\omega_1 = \omega_{min}$ in order to maintain its surge velocity. Improved turning performance is observed in the region between the flattened upper and lower curves.

Retained Data	
Course	Advance
	Transfer
	Tactical Diameter
	Turn Time
	Average Turn Rate
	Surge Velocity through the turn
Depth	Depth Overshoot
	Depth Rate
	10 m depth change time
	Surge Velocity through the turn
Surge Velocity	Steady State RPM
	Actual Speed
	Surge Velocity vs. Propeller RPM

Table 3-5: Retained data

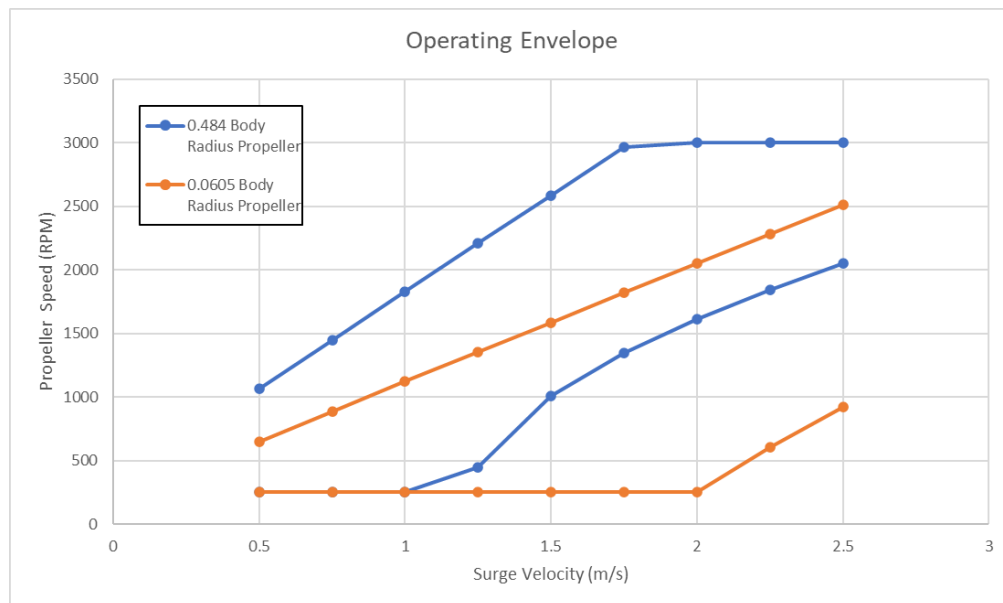


Figure 3-12: Operating Envelope example

3.6 Comparison model

Section 3.2.3 discusses the development of hydrodynamic coefficients for both the single bladed propeller actuated AUV and the conventional rudder and fin actuated AUV. This was done to provide a baseline comparison of the expected performance of

the single bladed actuated AUV relative to conventional actuation. This is done using the same PID control architecture for the equivalent pitch-heave and sway-yaw architecture but by replacing the PID coefficients with those listed in Table 3-6 and Table 3-7. In addition, the b matrix for sway-yaw and pitch-heave subsystems was replaced by equations 3.75 and 3.76 respectively. The hydrodynamic coefficients account for the force and moment effects generated by a change in angle of the rudder (sway-yaw subsystem) and fins (pitch-depth subsystem). The conventionally actuated AUV was then subjected to the same tests as the single bladed propeller actuated AUV and the Table 3-5 data was retrieved for comparison.

$$b = \begin{bmatrix} Y_{\delta} \\ N_{\delta} \\ 0 \end{bmatrix} \quad (3.75)$$

$$b = \begin{bmatrix} Z_{\delta} \\ M_{\delta} \\ 0 \end{bmatrix} \quad (3.76)$$

Sway-Yaw PID Controller Coefficients	
K_P	1.00
K_I	0.00
K_D	5.00

Table 3-6: Rudder sway yaw PID controller coefficients

Pitch Heave PID Controller Coefficients	
K_P Pitch	6.00
K_I Pitch	0.00
K_D Pitch	2.80
K_P Depth	0.50
K_I Depth	0.00
K_D Depth	0.00

Table 3-7: Fin pitch-heave PID controller coefficients

CHAPTER 4

RESULTS

4.1 Results of the propeller sizing procedure:

The first four steps of the overall Design Methodology for the single bladed propeller were accomplished by the parameters given in the design case study for the short hulled AUV discussed in section 3.1. The following sections focus on steps 5 and 6 for modeling the performance of the AUV to determine the optimum size of the propeller blade. The application of the Propeller Sizing Procedure validated the actual propeller blade size, 4.23 cm or 0.629 body radius, is sufficient for actuating the short hulled AUV. Its performance can be improved with a larger propeller but is limited by the incorporation of a shroud around the propeller. This will limit the propeller blade size to less than the inner diameter of the shroud.

4.1.1 Determine the propeller RPM as a function of blade length for design maximum speeds.

Figure 4-1 displays the relationship between the Propeller RPM and the steady state surge velocity produced the propeller. The blue vertical line indicates the design maximum speed threshold, and the orange vertical line indicates the design mission speed threshold. The different lines of best fit relate to a single bladed propeller blade size ranging from 0.446 Body Radius to 0.744 Body Radius. The resulting equation providing the Propeller RPM for a given single propeller blade size are listed in Table 4-1. This analysis revealed propeller blades less than 0.595 hull radius couldn't prove sufficient thrust to attain the design maximum surge velocity of 2.5 m/s.

The smallest propeller, the 0.446 body radius propeller couldn't reach the design mission speed as well. This removed the 0.446 and 0.521 hull radius propeller blades from further consideration in the coupled vehicle control tests. They are included in the uncoupled performance tests to better assess the capability of the single bladed propeller.

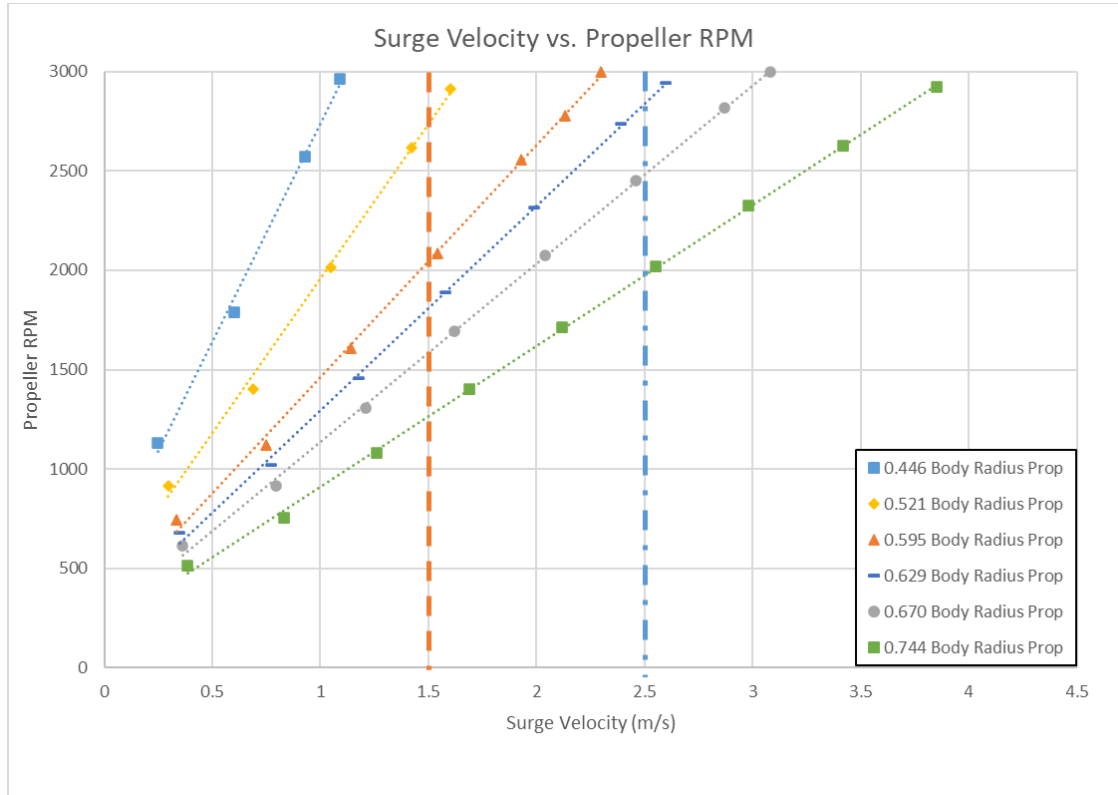


Figure 4-1: Surge velocity vs. propeller RPM for the short hulled test shape

Propeller Blade Size (Body Radius)	Surge Velocity to Propeller RPM Eq.
0.446	$RPM = 2189 * U + 543.9$
0.521	$RPM = 1557 * U + 398.7$
0.595	$RPM = 1165 * U + 299.1$
0.629	$RPM = 1026 * U + 270.7$
0.670	$RPM = 895.1 * U + 243.0$
0.744	$RPM = 708.9 * U + 203.0$

Table 4-1: Surge velocity to propeller RPM equations

4.1.2 Model advance, transfer, tactical diameter, and depth changing performance as a function of speed and propeller diameter

This design procedure step will be split into separate sections. The first section will focus on the results of the course changing open loop tests and the second section will focus on the depth changing open loop tests.

4.1.2.1 Modeling advance, transfer, and tactical diameter

The maneuvering performance tests described in sections 3.4.2 were conducted by applying a 180 degree course perturbation to the single bladed AUV. Figure 4-3 shows the best achievable turning characteristics for propeller blade sizes ranging from 0.446 to 0.744 hull radius and Figure 4-4 shows the turning time. The best achievable turning characteristics were obtained by conducting maneuvering tests with the maximum possible $\omega_{diff} = 2750 \text{ RPM}$. The tests were conducted at the “ideal” turning speed. The “ideal” turning speed was found by finding ω_{avg} for the 3000 and 250 RPM. The ω_{avg} was used to calculate the corresponding steady state surge velocity or the “best” turning speed. The “ideal” turning speed is depicted in Figure 4-2 for each propeller blade size. It appears the “ideal” turning speed occurs between 40-80% of the short hulled test shape’s design speed, 2.5 m/s.

The 0.446 and 0.521 propeller blades provided smaller maneuvering characteristics but this is likely due there lower “ideal” turning speeds as indicated by their long turn times. A propeller blade size from 0.595 to 0.744 body radius resulted in similar maneuvering characteristics but reduced turning time as the propeller blade size increased. This seems to indicate the maneuvering characteristics are limited by

the vehicle hydrodynamics but the best turning speed is improved by a larger propeller blade.

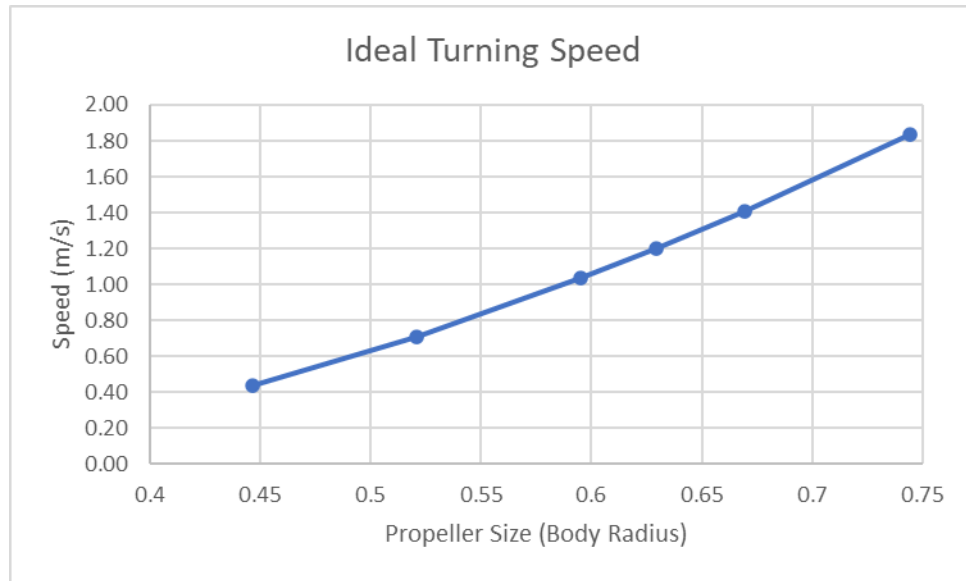


Figure 4-2: Ideal turning speed

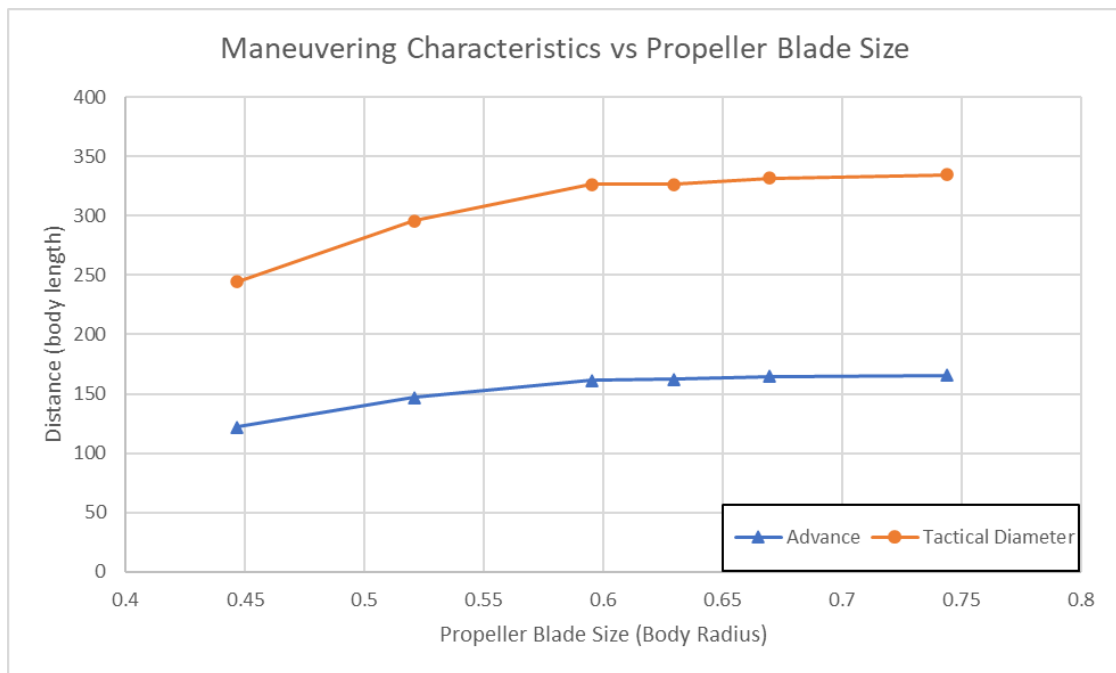


Figure 4-3: Maneuvering characteristics vs. propeller blade size

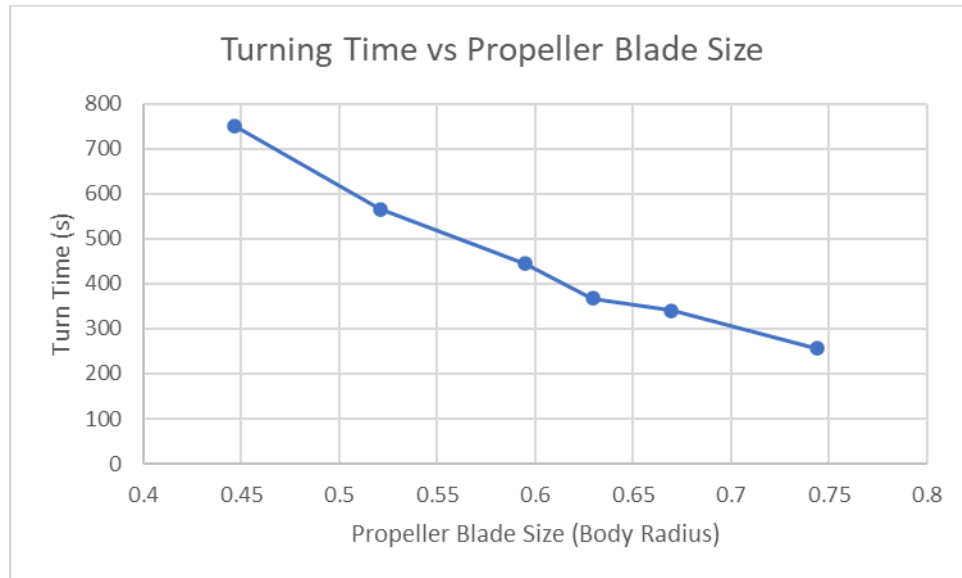


Figure 4-4: Turning time vs propeller blade size

4.1.2.2 Modeling depth changing performance

The depth performance tests used the same “best” turning speeds per Table 4-2. Figure 4-5 shows the relationship between the Depth Overshoot and Propeller Blade Size. Figure 4-6 shows the relationship between the Depth Changing Time and Propeller Blade Size. In general, increasing blade size improves the ability of the AUV to change depth. This follows a similar trend where to the preceding section where a using a larger propeller blade resulted in improved performance.

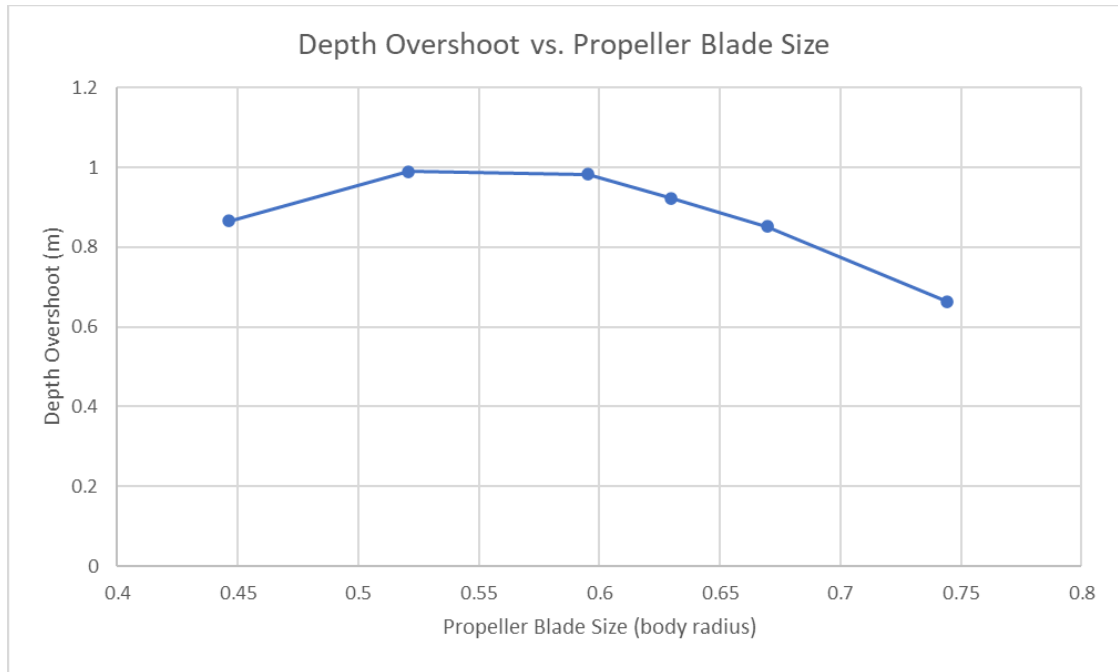


Figure 4-5: Depth overshoot vs. propeller blade size

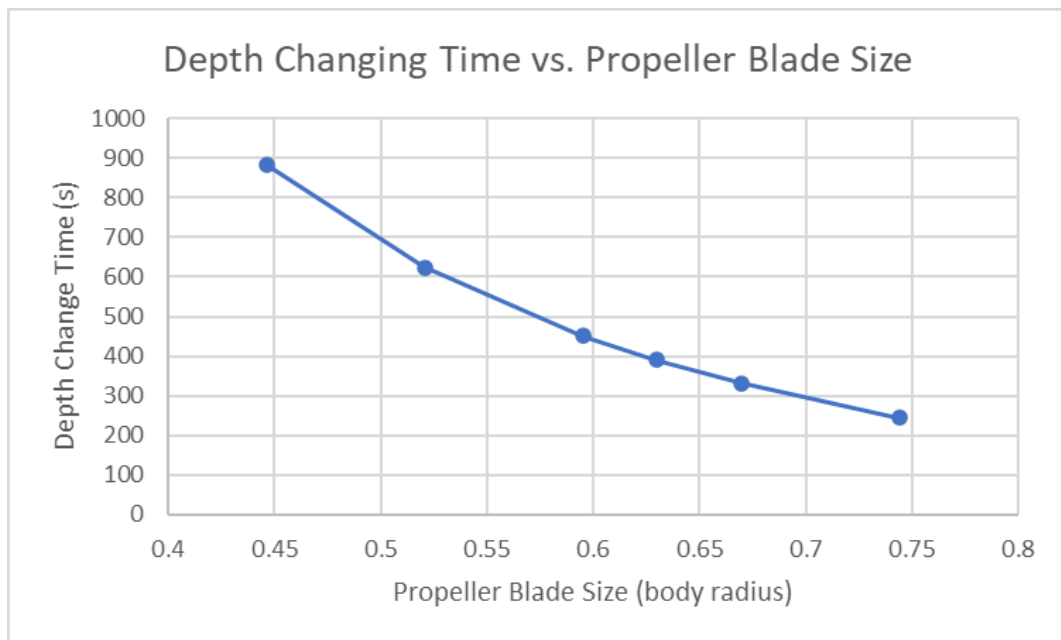


Figure 4-6: Depth change time vs. propeller blade size

4.1.2.3 Propeller angular velocity differential tests

The effect of varying the allowable angular velocity difference is displayed in Figure 4-7. The allowable angular velocity difference has a major effect on the maneuvering performance of the single bladed propeller actuated AUV. At differences less than 1000 RPM, all maneuvering characteristics are substantially higher. There is minimal improvement in the maneuvering characteristics at allowable angular velocity differences greater than 1500 RPM. This indicates a greater propeller angular velocity difference enhances maneuvering performance but only so much.

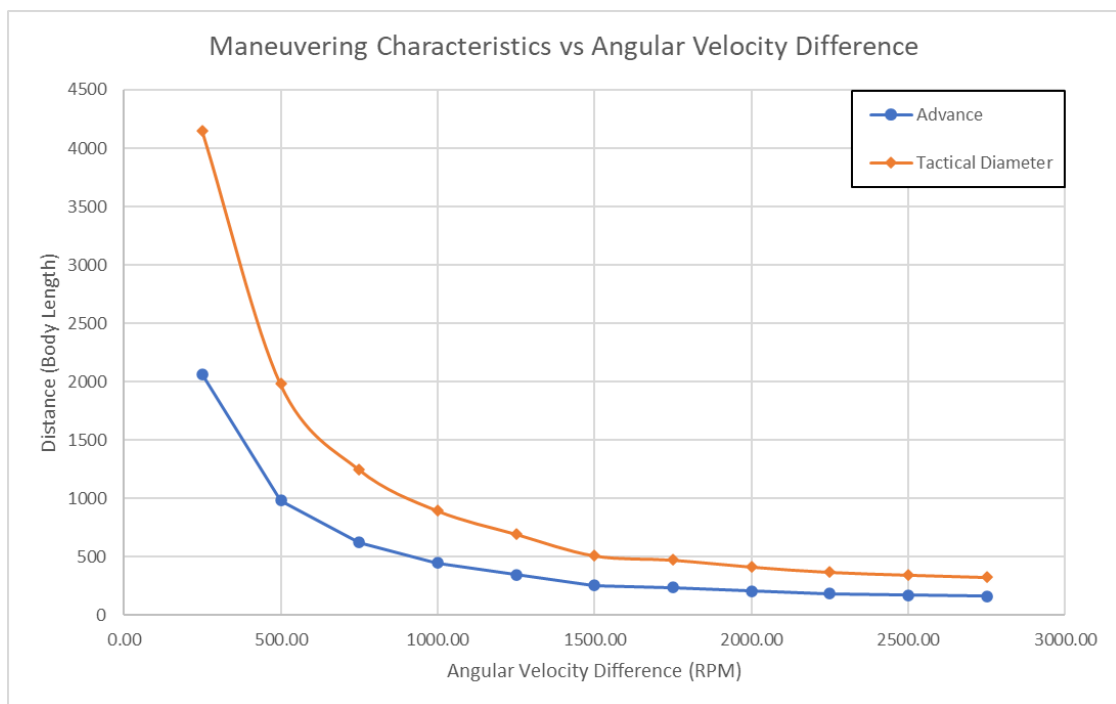


Figure 4-7: Maneuvering characteristics vs. angular velocity difference

4.1.2.4 Coupled maneuvering dynamic tests

The coupled maneuvering cases were completed for the next phase of analysis. The 0.446 and 0.521 body radius propellers had been removed from consideration.

They could not meet the design maximum speed for the short hulled AUV. While they could achieve the desired changes in course and depth their ability, their ability to generate a pitch or yaw moment able to accomplish a simultaneous depth and course change was doubtful.

It was assessed the best way to determine the effects on the coupled maneuvering characteristics was to conduct multiple tests across arrange of propeller blade sizes from 0.595 to 0.744 body radius and then compare how much the maneuvering characteristics increased. The tests were conducted from 0.5 m/s to 2.5 m/s. Figure 4-8 displays the maneuvering curves for the short hulled AUV using its designed 0.595 hull radius propeller under four conditions at 1.5 m/s: Case 1: rudder actuated, Case 2: single bladed propeller no surge velocity control, Case 3: single bladed propeller with surge velocity control, and Case 4: single bladed propeller, surge velocity controlled, and a depth excursion. These cases are summarized in Table 4-2 and the tracks were overlaid in Figure 4-9. 1.5 m/s was chosen for the test speed because it was the short hulled AUV's design cruise/mission speed and later analysis revealed it was contained within the single bladed propeller's ideal operating point. This "ideal operating point" will be discussed later in this chapter. The course maneuvering capability was chosen to compare the single bladed propeller to rudder because it required the most control input to achieve the full 180 degree turn. The rudder was included in this analysis to provide a baseline for comparison for the single bladed propeller's capabilities and will be discussed later in the results portion.

Case Number	Case Description
1	Rudder Actuated
2	Single Bladed Propeller Actuated No Surge Velocity Control
3	Single Bladed Propeller Actuated Surge Velocity Control
4	Single Bladed Propeller Actuated Surge Velocity Control and Depth Perturbation

Table 4-2: Test case description

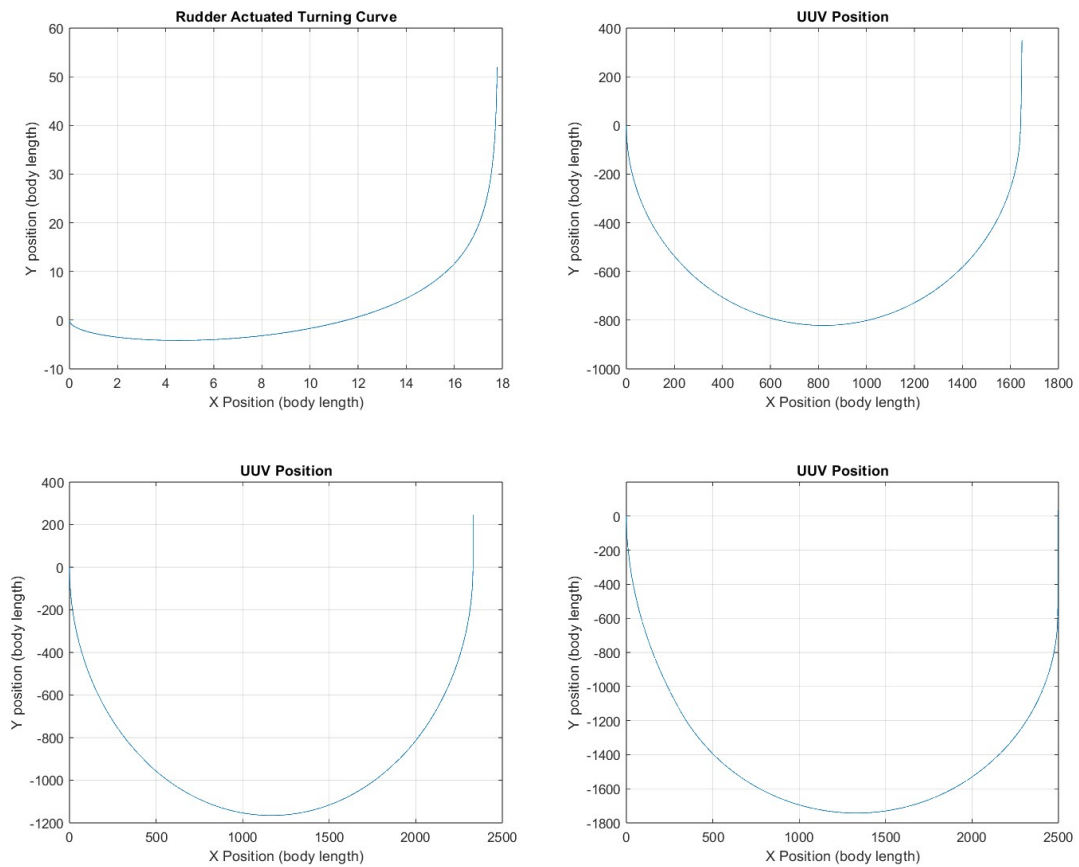


Figure 4-8: AUV maneuvering curves: case 1(upper left), case 2 (upper right), case 3 (lower left), case 4 (lower right)

4.1.2.5 Coupled controller performance degradation

There is substantial performance degradation for the single bladed propeller when control is coupled in anyway. Figure 4-8, Figure 4-9, and Table 4-3 shows the effect on the course open loop response for several cases. As more control authority is demanded by the other controllers, the ability of the propeller to respond to a change in any one DOF is reduced. This is due to the fixed maximum moment and thrust produced by the single bladed propeller.

	Case 1	Case 1 to 2 Change	Case 2	Case 2 to 3 Change	Case 3	Case 3 to 4 Change	Case 4
Advance (Body Length)	4.17	5977%	253.4	360%	1165	50%	1743
Transfer (Body Length)	4.53	5476%	252.6	379%	1210	10%	1330
Tactical Diameter (Body Length)	17.81	2754%	508.3	359%	2331	7%	2496
Time to turn 180 deg (s)	32.5	1281%	449	320%	1886	18%	2228
Average Turn Rate (Deg/s)	5.54	-93%	0.400	-75%	0.100	-20%	0.080

Table 4-3: Course changing performance degradation

The largest change is from the incorporation of speed control which results in a 359% to 379% larger turning characteristics. The column highlighted in red for Case 2 and Case 2 to 3 indicates the effects of incorporating speed control to the AUV maneuvers. Case 1 is the maneuvering characteristics due to the effects of the rudder. The change of Case 1 to Case 2 is very substantial indicating the propeller is less effective than the rudder. However, since the rudder data is the control case, the change from Case 2 to Case 3 is the focus for this analysis. The incorporation of speed control reduces the maximum yaw or pitch moment which can be produced by the

single bladed propeller. This substantially affects the turning and depth changing performance of the AUV and prevents achieving maximum turning performance or performance comparable to a conventional rudder and stern planes. Figure 4-9 shows the four plots in Figure 4-8 overlaid on each other showing the change in scale as each maneuvering case is developed. The difference between Case 1 and Case 2 was immense and a separate plot was made to depict the change in maneuvering characteristics in Figure 4-9.

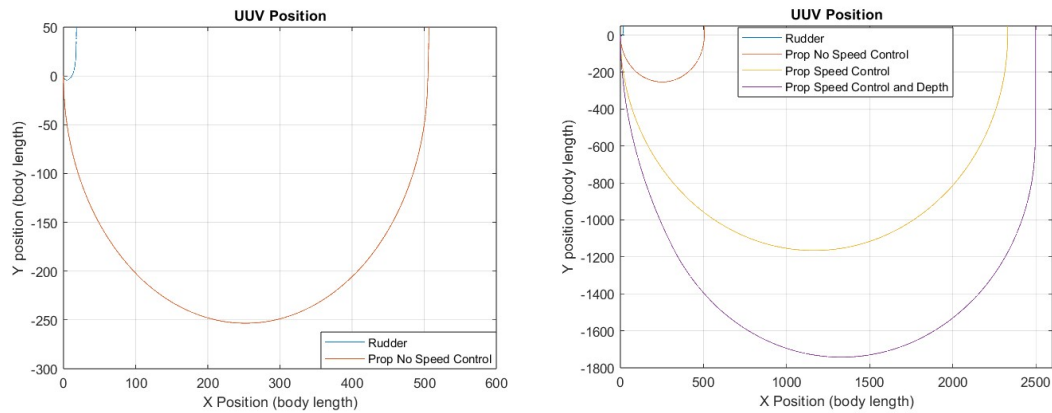


Figure 4-9: Case 1-4 overlaid plots (right), Rudder and Propeller No Speed Control overlaid (left).

Depth control incorporation results in a 50% increase in the advance, and 10 to 7% increase in the transfer and tactical diameter. The depth control coupling doesn't result in as large of a decrease in performance as surge velocity control coupling. A 10 m depth change is relatively small compared to the 180 degree course change and is accomplished in the first third of the total transient. This accounts for the most significant increase in the advance since less force is initially available to change the Short Hulled UUVs heading. Once the depth change is complete, the UUV applies the full actuation moment by the propeller to change course resulting the less

significant change in the transfer and tactical diameter. The reduction in yaw moment is experienced by the AUV for less time than surge velocity coupling reducing the relative impact of the depth control coupling. This effect will grow as the magnitude of the required course/depth change increases. The results of these coupled maneuvering tests reveal a larger propeller will typically provide better maneuvering characteristics due to the greater thrust generated by the propeller.

4.1.2.6 Operating region and propeller blade size

Figure 4-10 provides a depiction of the Turn Time vs. the Surge Velocity of the AUV. In the case of the short hulled AUV, the operating region appears to occur between 1-2 m/s based on the propeller size. Also, a larger propeller blade size results in a larger operating region. At lower speeds, this occurs due to the maximum ω_2 being reduced to maintain the low speed. At higher speeds, this occurs due to the limited ω_{diff} available while the AUV attempts to maintain surge velocity while changing course or depth. The 1.5 m/s test speed used to generate Figure 4-8 is within the operation of the propeller blade sizes tested as part of this design process.

The operating region should be designed where it encompasses the optimal transit and survey speeds required for the AUV's primary missions. However, this could result in difficulty for the AUV to complete missions with high current as it MUST operate in this region to maximize maneuverability.

This could result in an optimal propeller blade with a longer span than the hull radius required to produce the desired maneuvering performance. However, the propeller size can be limited by other factors such as a size limitation for the AUV. It is advantageous for the propeller and a shroud assembly (if installed) to have the same

diameter as the rest of the AUV hull. This minimizes axial drag and simplifies design of the carriage tube or case for an AUV. The propeller size is the primary means to improve the performance of an AUV using a single bladed propeller.

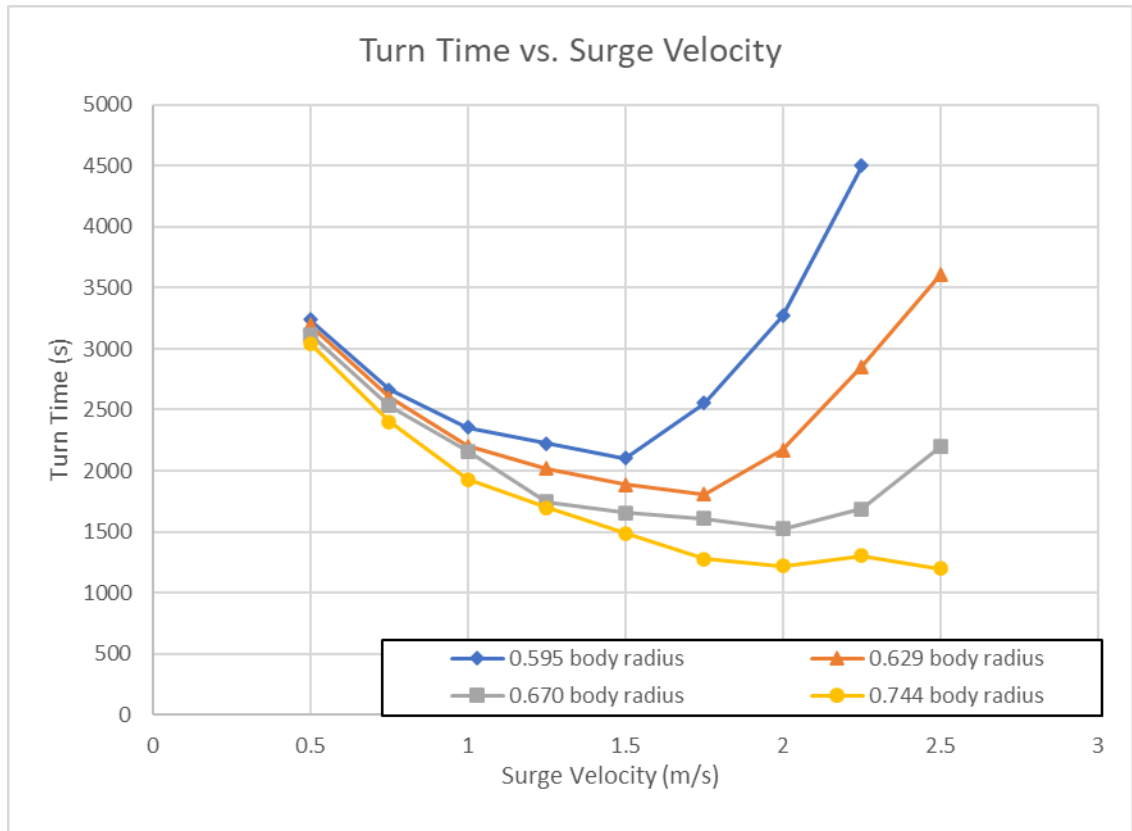


Figure 4-10: Turn time vs. surge velocity

4.2 Based on the modeling and simulation results select the optimum propeller blade length to meet design requirements.

Figure 4-11 depicts the operating envelope of the AUV while surge velocity control is established. Improved turning performance is observed in the region between the flattened upper and lower curves. The 0.595 body radius propeller appears to have its improved turning performance between 1.00 and 1.75 m/s. The 0.744 body radius propeller appears to have its improved turning performance between 1.75 m/s and 2.5 m/s based on the graphic. The lower curve for both propeller blade sizes occurs at the 250 RPM minimum propeller angular velocity. The 0.595 body radius propeller achieves the maximum propeller angular velocity at 1.75 m/s indicated by the horizontal upper curve. The UUV propelled by the 0.595 body radius propeller is saturated between maintaining depth, course, and speed above 1.75 m/s. The 0.744 body radius propeller never achieves the maximum propeller angular velocity indicating the saturation surge velocity occurs higher than the design maximum speed of the AUV. This shows how the operating region of the AUV shifts to higher surge velocities with a larger propeller and indicates the improved performance at those higher speeds.

The 0.595 and 0.744 body radius propellers provide the upper and lower bound for suitable short hulled AUV propellers based on the analysis completed in section 4.1, the design mission and maximum speed and Figure 4-10. The 0.595 body radius propeller provides the minimum expected performance of the AUV by providing a maximum speed ~ 2.25 m/s (10% less than the design maximum speed) and maneuvering characteristics comparable to larger propeller blades per Figures 4-3 and

4-4. The 0.595 body radius has an operating region between 1.0 and 1.75 m/s with a “best” turning speed of 1.04 m/s. However, there is room for a larger propeller blade up to 0.744 body radius. The 0.744 body radius propeller blade provides better turning rates and improves the ability of the AUV to handle compound speed, course, and depth perturbations. Its “ideal” turning speed is around 1.84 m/s which can result at less desirable performance at the design mission speed of 1.5 m/s. The larger operating region for the 0.744 body radius propeller at higher speeds provides similar or better performance than the 0.595 body radius propeller while operating at a lower propeller RPM. A propeller 0.744 body radius may require the propeller extending past the hull or requiring a larger shroud. In addition, it will result in higher resistive torque acting on the motor. In both cases, this will reduce the efficiency of the AUV. While a smaller propeller than 0.595 body radius will result in reduced performance. The current short hulled AUV propeller blade size of 0.629 body radius is inside the optimum propeller blade size range and provides the required performance. Therefore, the existing single bladed 0.629 body radius propeller is sufficient for the short-hulled test shape.

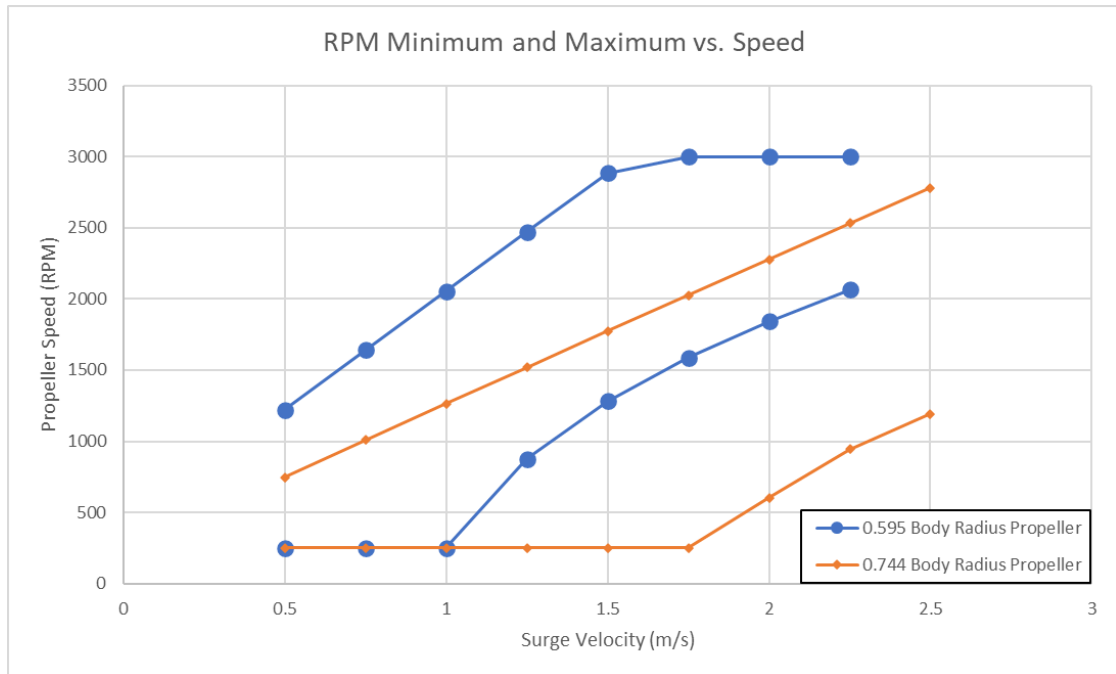


Figure 4-11: Short hulled AUV operating envelope

4.3 Additional results

4.3.1 Single bladed propeller vs. rudder performance

The single bladed propeller can obtain performance within two orders of magnitude to a rudder without a speed controller instituted. However, it struggles to even approach the performance achieved by a rudder. Previous literature indicates the propeller can achieve similar performance and maneuverability [10], [12] but this is not the case in these results as shown in Figure 4-8, Figure 4-9, and Table 4-3. This gap in performance could be achieved by using a larger motor than with a higher peak RPM to maximize the yaw or pitch moment. Armada Robotics [2] provides an alternative method where the AUV is directed to conduct multiple back and forth movements to change direction in a small location. This is an interesting concept but was not tested as part of the bounds of this thesis and is indicative of the low-speed maneuverability of the one bladed propeller.

4.3.2 Shroud effectiveness

The actual short-hulled test shape and single bladed propeller assembly produced by Armada Robotics incorporates a shroud around the propeller. The incorporation of the shroud may increase the thrust of the single bladed propeller up to 60%-68% at the low speeds used by most AUVs [14], [9] at a given propeller angular velocity compared with an unshrouded propeller. Additional course changing runs were conducted at 1.5 m/s to account for the increase in thrust due to the shroud.

The tests were conducted at the as built “short hulled” AUV propeller blade size of 0.629 body radius. Figure 4-12 shows an increase in the maximum surge velocity achieved by the AUV. Table 4-4 shows the maximum surge velocity achieved by each propeller blade length compared and the percent difference between the maximum velocities achieved with and without the shroud. In all cases, the incorporation of the shroud improved the surge velocity achieved by the single bladed propeller up to 38.1%. This is due to the increased thrust provided by the propeller shroud. This indicates the incorporation of thrust improving devices can substantially improve performance of the single bladed propeller.

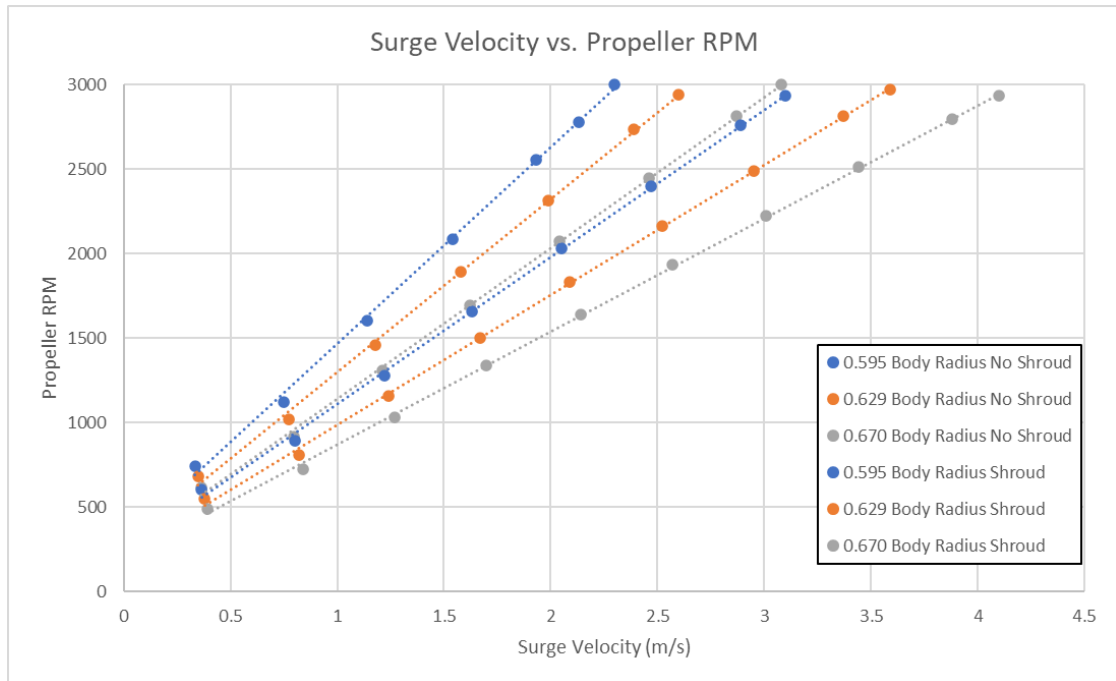


Figure 4-12: Impact of the propeller shroud on surge velocity performance

Shroud Impact on Maximum Surge Velocity			
Propeller Blade Size (Body Radius)	Unshrouded Maximum Velocity (m/s)	Shrouded Maximum Velocity (m/s)	Percent Increase
0.595	2.30	3.10	34.8%
0.629	2.60	3.59	38.1%
0.670	3.08	4.10	33.1%

Table 4-4: Shroud impact on maximum surge velocity

Figure 4-13 and Table 4-5 depict the difference in the maneuvering parameters between the shrouded and unshrouded short hulled UUV. The additional thrust from the shroud resulted in a reduction in the advance, transfer, and tactical diameter turning parameters performed at the ideal operating speed with surge velocity control removed. Figure 4-13 depicts a shift in the short hulled UUVs ideal operating region from 1 m/s to 1.75 m/s with no shroud thrust contribution to 1 to >2.5 m/s with the shroud thrust contribution. These results indicate the shroud can substantially increase performance of the AUV by 38-60%. However, other methods may be required to

improve the performance of the single bladed propeller to approach the performance of a conventional rudder and fins.

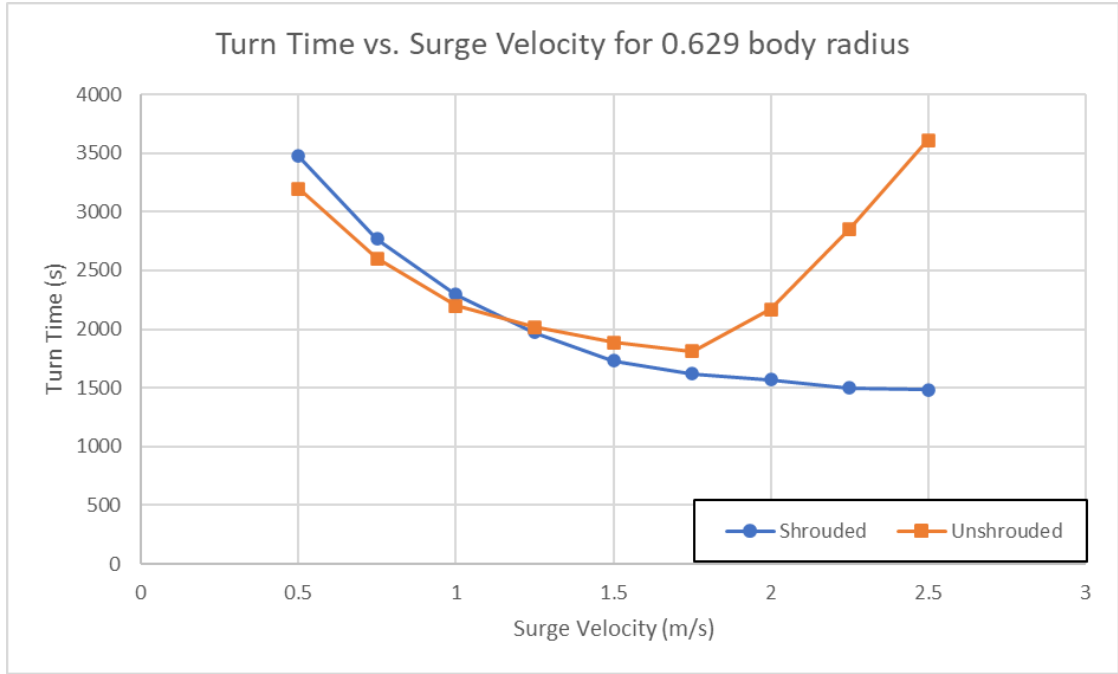


Figure 4-13: Turn time vs. surge velocity comparing shrouded and unshrouded short hulled UUV performance

	Unshrouded	Shrouded	Percent Change
Advance (Body Length)	253.4	152.1	-39.98%
Transfer (Body Length)	252.6	150.9	-40.28%
Tactical Diameter (Body Length)	508.3	306.7	-39.65%
Time to turn 180 deg (s)	448.5	275.0	-38.68%
Average Turn Rate (Deg/s)	0.40	0.65	63.07%

Table 4-5: Change in UUV maneuvering performance at 1.5 m/s based on incorporation of the shroud

4.4 Identified Limitations

The application of the propeller sizing procedure provided a means to quickly iterate and refine the propeller blade sizes. The procedure also identifies the major limitation for the single bladed propeller which is the coupled nature of the vehicle dynamics. The single bladed propeller can successfully change AUV course, depth, and speed but not as effectively as a conventional propeller, fins, and rudders combination. The best maneuvering capability requires using the maximum available ω_{diff} based on the lowest allowable propeller RPM and the maximum RPM of the motor. This will result in the AUV accelerating or deaccelerating whilst attempting a fast depth or course change if it is not already operating at its “best” turning speed. On the other hand, incorporating surge velocity control precludes the AUV from achieving its maximum performance.

Another minor concern is noted in videos produced by Armada Robotics [2]. In each example, a substantial amount of roll is induced by the modulation of the single bladed propeller speed. However, this can be mitigated by enhancing passive stability by lowering the center of gravity below the center of buoyancy through careful weight placement and management [7], [14] which is already a recognized technique for improving roll resistance.

CHAPTER 5

CONCLUSIONS AND FUTURE WORK

5.1 Design methodology

The single bladed propeller provides a viable, versatile, and a mechanically simple solution for AUV actuation. It can provide sufficient maneuvering performance for AUV applications to meet the necessary requirements for research institutions. It is also capable of dynamic positioning at slow speeds through use of its single bladed propeller [12]. However, designing an AUV to use this propulsion method requires specific design considerations and optimize its performance. The design methodology presented in section 1.2 is effective for ensuring the single bladed propeller characterization is conducted to aid in system design. It provides a logical and straightforward process for optimizing the propeller blade size for a specific application. The following sections lay out the single bladed propeller specific design considerations and limitations developed while applying the design methods described in section 1.2.

5.1.1 Design considerations

The single bladed propeller requires some specific design considerations for its implementation. The design considerations include its “operating region”, propeller blade size restrictions, drive motor selection, and desired performance. The desired performance is simply the engineering requirement for the design and its maneuverability. The “operating region” is the speeds where the AUV can obtain maximum maneuverability while requiring a fixed surge velocity during a maneuver. The dominant variable for performance is the length of the propeller blade.

The design methodology laid out in this thesis indicates changes even as small as 0.5 cm is sufficient to improve or reduce performance of the single bladed propeller. Therefore, a small range of suitable propeller blade sizes can be developed for consideration to balance engineering requirements with size constraints. While a larger propeller results in greater maneuverability, oversizing the propeller can result in a cumbersome AUV layout or a less efficient propeller. A secondary method could be to use a more powerful motor which enables a higher operating angular velocity permitting a greater difference in propeller angular velocity.

5.1.2 Limitation mitigation

As discussed in Chapter 4, there appears to be an optimum operating region midway between the 0 and the maximum operating speed of the AUV. Analysis of the “short hull test shape” determined it had its optimum operating region between 1.25 - 1.75 m/s. The propeller could generate sufficient average thrust to maintain surge velocity while maximizing ω_{diff} within this operating region. In addition, it can achieve similar maneuvering performance to a similar rudder or control fin actuated AUV without surge velocity control. The AUV operator can mitigate this performance degradation through route and speed planning. In a traditional “mow the lawn” survey track pattern, the AUV may need surge velocity control while on a survey track but could remove the surge velocity control while setting up for the next survey leg. It is ideal to optimize the AUVs sensors for use at a surge velocity within its operating region.

The coupled depth and course dynamics can potentially be solved by incorporating control parameter prioritization logic. This will enable the AUV to

automatically select whether to prioritize achieving the required depth and speed based on its relative magnitude or by attaching a priority scheme to the track plan.

A roll perturbation will be applied to the AUV every time it modulates drive motor output due to the asymmetric thrust from the propeller thrust. This could preclude precision surveys where minimal roll is desired by the AUV. However, it can be potentially mitigated by ballasting the AUV in such a way to provide passive roll stability to overcome the propeller perturbations.

5.2 Recommendations for future work

5.2.1 Physical model verification

This thesis is focused on modeling and simulation. It has yet to be validated with physical tests. A natural next step would be to observe the performance of the short hull test shape and validate the models. This would also permit adjusting the viscous drag coefficients to better match actual vehicle performance. In the interim, it is possible to better estimate the added mass and viscous drag coefficients using the computational fluid dynamics (CFD) as outlined in [11]. CFD appears to be a valid method for estimating hydrodynamic coefficients for the vessel.

Another next step for the single bladed propeller would be to develop nonlinear Hydrodynamic coefficients for updated modeling and simulation efforts. This would better approximate the highly coupled dynamics of the single bladed propeller actuated AUV. However, it appears at slow speeds the coupled linear models provide good enough performance. This can only be validated through further analysis of the actual physical model.

5.2.2 Roll susceptibility analysis

After inspection of Armada Robotics media [2] it was determined the modulated output of the single bladed propeller imparts substantial roll dynamics to the AUV. This could be a potentially limiting factor for the single bladed propeller application as it could preclude use of side scan or multi beam sonars preventing its use for survey missions. In addition, it could require some added design passive or active roll dampening which could add sufficient cost to render the single bladed propeller cost ineffective for survey applications. This is a key concern which should merit additional modeling and analysis but was beyond the scope of this study.

5.2.3 Path following capability analysis

This thesis focused heavily on open loop for large course and depth changes for the AUV with a focus on its capabilities relative to a conventional AUV design. It did not model the ability of the single bladed propeller to maintain the AUV course and depth on a required path. This test is also necessary for optimizing the vehicles course and depth controllers for its mission. Substantial work has been done [7], [21], and [25] on other control algorithms to improve vehicle control. Similar tests should be done with this propulsion concept to assess its ability to follow its path and conduct missions. Later follow on research could aid in determining the optimum control architecture for this propulsion concept. Figure 5-2 depicts an example of a spiral trajectory tracking used by Thanh, Tam, and Anh to assess the performance of their control system [24]. A similar control trajectory could be used to assess the ability of the single bladed propeller to maintain its path.

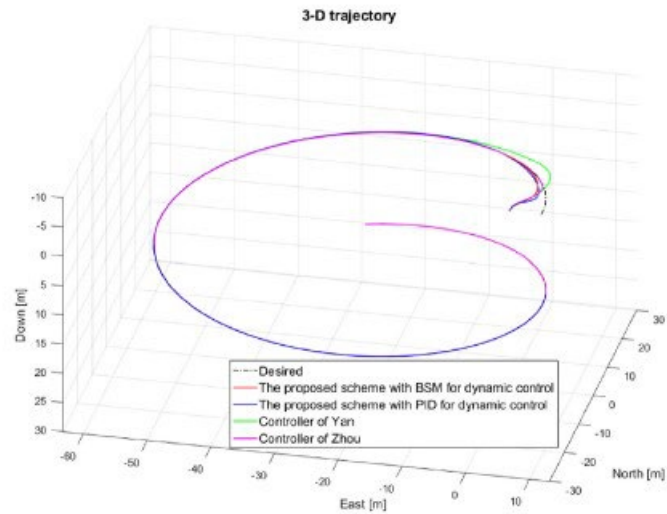


Figure 5-1: Example path following test [24]

5.2.4 Long term pitch control

The single bladed propeller by design does not use a set of fins to change pitch angle and depth. This reduces the number of actuators for the AUV however it can make depth control more difficult in practice. A conventional undersea vehicle can set its pitch angle using its fins. The lift on the vehicle hull and the fins will enable the AUV to overcome the reserve buoyancy trimmed into the AUV to aid recovery. The result is the vehicle hull may not move at all while fins oscillate to maintain depth. The single bladed propeller will need to constantly modulate its propeller output to change the pitch angle and the lift acting on the vehicle. This could have an adverse effect on depth control resulting the hull pitch angle oscillating to maintain depth reducing the quality of the AUVs mission data. This could make it difficult for the AUV to maintain a fixed depth through changing water densities at different points in the water column. In addition, this increases the settling time of the AUV at a new

depth reducing its ultimate depth changing performance. This concern is seen in the depth control tests where depth and pitch angle go through several oscillations before settling at their final values.

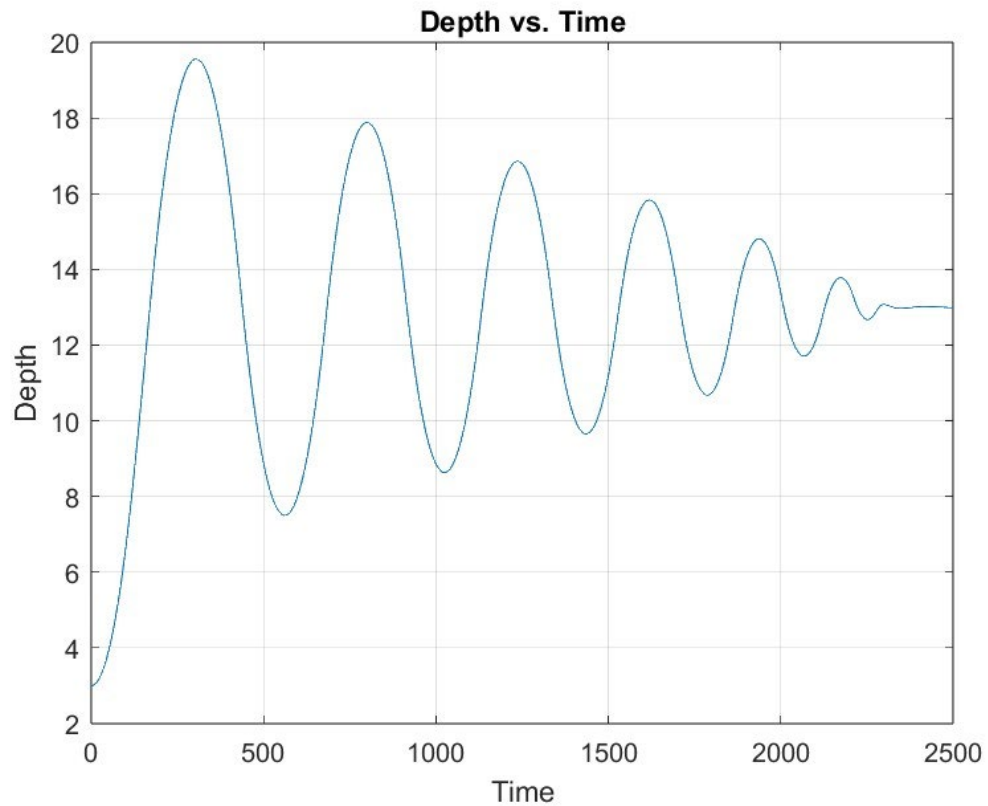


Figure 5-2: Depth control oscillation example

If the depth control becomes particularly limiting, this may require incorporation of a slow period pitch control system to maintain a fixed pitch angle whilst the AUV conducts a mission. This could take the form of a weight on a worm driven actuator to shift the center of gravity of the AUV to provide longitudinal stability.

5.2.5 Control authority allocation and prioritization

A compound course, depth, or surge velocity perturbation would need some form of actuator output prioritization based on mission parameters to minimize affects in coupled dynamics. Algorithms laid out in Salumäe [21] provides an example of a solution for an AUV using biomimetic propulsion approximating a sea turtle.

There is some literature available for biomimetic propulsion [21] which applies the concept of control priority management. The DOF prioritization strategy works by assigning priorities to the control actions using smoothing functions [5], [21]. Equation 5.1 is applied to the input vector to weight the input. The sum of the 6 vector components is equal to 1. In the case of the single bladed propeller concept, this control can be simplified for priority values for the course, depth, and surge velocity error.

$$p = [p_x, p_y, p_z]^T \quad (5.1)$$

The allocation of propeller control output is indirectly included in the steering angle calculation in equation 3.34 for optimizing yaw and pitch control based on magnitude of the respective perturbation using logic from [10]. However, it results in the AUV applying a steering angle providing yaw and pitch moments with the same magnitude to correcting a simultaneous depth and course perturbation. This results in the AUV correcting the smallest perturbation first since less time would be required to correct it than a larger perturbation with the same magnitude moment. This tendency indicates some form of control authority allocation or prioritization may be required to enhance single bladed propeller performance. Additional study is recommended for applying this concept.

APPENDICES

Appendix A: Mass matrix data

Single Bladed Propeller Prolate Spheroid Approximation

$$\mathbf{M} = \begin{bmatrix} m_{11} & m_{12} & m_{13} & m_{14} & m_{15} & m_{16} \\ m_{21} & m_{22} & m_{23} & m_{24} & m_{25} & m_{26} \\ m_{31} & m_{32} & m_{33} & m_{34} & m_{35} & m_{36} \\ m_{41} & m_{42} & m_{43} & m_{44} & m_{45} & m_{46} \\ m_{51} & m_{52} & m_{53} & m_{54} & m_{55} & m_{56} \\ m_{61} & m_{62} & m_{63} & m_{64} & m_{65} & m_{66} \end{bmatrix} = \begin{bmatrix} 7.44 & 0.00 & 0.00 & 0.00 & 0.00 & 0.00 \\ 0.00 & 7.44 & 0.00 & 0.00 & 0.00 & 0.00 \\ 0.00 & 0.00 & 7.44 & 0.00 & 0.00 & 0.00 \\ 0.00 & 0.00 & 0.00 & .013 & 0.00 & 0.00 \\ 0.00 & 0.00 & 0.00 & 0.00 & .031 & 0.00 \\ 0.00 & 0.00 & 0.00 & 0.00 & 0.00 & .031 \end{bmatrix}$$

$$\mathbf{M}_a = \begin{bmatrix} m_{11} & m_{12} & m_{13} & m_{14} & m_{15} & m_{16} \\ m_{21} & m_{22} & m_{23} & m_{24} & m_{25} & m_{26} \\ m_{31} & m_{32} & m_{33} & m_{34} & m_{35} & m_{36} \\ m_{41} & m_{42} & m_{43} & m_{44} & m_{45} & m_{46} \\ m_{51} & m_{52} & m_{53} & m_{54} & m_{55} & m_{56} \\ m_{61} & m_{62} & m_{63} & m_{64} & m_{65} & m_{66} \end{bmatrix} = \begin{bmatrix} .591 & 0.00 & 0.00 & 0.00 & 0.00 & 0.00 \\ 0.00 & 7.07 & 0.00 & 0.00 & 0.00 & -.224 \\ 0.00 & 0.00 & 7.07 & 0.00 & .224 & 0.00 \\ 0.00 & 0.00 & 0.00 & .009 & 0.00 & 0.00 \\ 0.00 & 0.00 & .224 & 0.00 & .219 & 0.00 \\ 0.00 & -.224 & 0.00 & 0.00 & 0.00 & .219 \end{bmatrix}$$

Fin Actuated Prolate Spheroid Approximation

$$\mathbf{M} = \begin{bmatrix} m_{11} & m_{12} & m_{13} & m_{14} & m_{15} & m_{16} \\ m_{21} & m_{22} & m_{23} & m_{24} & m_{25} & m_{26} \\ m_{31} & m_{32} & m_{33} & m_{34} & m_{35} & m_{36} \\ m_{41} & m_{42} & m_{43} & m_{44} & m_{45} & m_{46} \\ m_{51} & m_{52} & m_{53} & m_{54} & m_{55} & m_{56} \\ m_{61} & m_{62} & m_{63} & m_{64} & m_{65} & m_{66} \end{bmatrix} = \begin{bmatrix} 7.44 & 0.00 & 0.00 & 0.00 & 0.00 & 0.00 \\ 0.00 & 7.44 & 0.00 & 0.00 & 0.00 & 0.00 \\ 0.00 & 0.00 & 7.44 & 0.00 & 0.00 & 0.00 \\ 0.00 & 0.00 & 0.00 & .275 & 0.00 & 0.00 \\ 0.00 & 0.00 & 0.00 & 0.00 & .323 & 0.00 \\ 0.00 & 0.00 & 0.00 & 0.00 & 0.00 & .323 \end{bmatrix}$$

$$\mathbf{M}_a = \begin{bmatrix} m_{11} & m_{12} & m_{13} & m_{14} & m_{15} & m_{16} \\ m_{21} & m_{22} & m_{23} & m_{24} & m_{25} & m_{26} \\ m_{31} & m_{32} & m_{33} & m_{34} & m_{35} & m_{36} \\ m_{41} & m_{42} & m_{43} & m_{44} & m_{45} & m_{46} \\ m_{51} & m_{52} & m_{53} & m_{54} & m_{55} & m_{56} \\ m_{61} & m_{62} & m_{63} & m_{64} & m_{65} & m_{66} \end{bmatrix} = \begin{bmatrix} 0.591 & 0.00 & 0.00 & 0.00 & 0.00 & 0.00 \\ 0.00 & 7.32 & 0.00 & 0.00 & 0.00 & -0.068 \\ 0.00 & 0.00 & 7.32 & 0.00 & .068 & 0.00 \\ 0.00 & 0.00 & 0.00 & .011 & 0.00 & 0.00 \\ 0.00 & 0.00 & .068 & 0.00 & .160 & 0.00 \\ 0.00 & -0.68 & 0.00 & 0.00 & 0.00 & .160 \end{bmatrix}$$

Appendix B: Hydrodynamic and Damping Coefficients (at 1.5 m/s)

Coefficient	Value
$M_{\dot{q}}$	-0.2190
$M_{\dot{w}}$	-0.2240
$N_{\dot{r}}$	-0.2190
$N_{\dot{v}}$	0.2240
$X_{\dot{u}}$	-0.5910
$Z_{\dot{q}}$	-0.2240
$Z_{\dot{w}}$	-7.067
$Y_{\dot{r}}$	0.2240
$Y_{\dot{v}}$	-7.067
M_q	-3.056
M_W	1.490
N_r	-2.379
N_v	11.75
X_u	0.07440
Z_q	0.5280
Z_w	-80.73
Y_r	0.5280
Y_v	-80.73

Appendix C: Course changing open loop test data

Rudder Actuated

Prop Size (cm)	Rudder	Rudder	Rudder	Rudder	Rudder
Test Speed (m/s)	0.50	1.00	1.50	2.00	2.50
Advance (body length)	1.75	2.92	4.17	5.45	6.74
Transfer (body length)	1.39	2.96	4.53	6.1	7.68
Tactical Diameter (body length)	5.74	11.8	17.8	23.8	29.9
Time to 180 turn (s)	30.4	31.2	32.5	31.3	32.7
Average Turn Rate (deg/s)	5.93	5.78	5.54	5.75	5.51
Omega 2 (RPM)	N/A	N/A	N/A	N/A	N/A
Omega 1 (RPM)	N/A	N/A	N/A	N/A	N/A
Omega Diff (RPM)	N/A	N/A	N/A	N/A	N/A
Avg RPM	N/A	N/A	N/A	N/A	N/A

No Speed Control – Unshrouded Propeller

Prop Size (body radius)	0.446	0.521	0.595	0.629	0.670	0.744
Omega Diff (RPM)	2750	2750	2750	2750	2750	2750
Best Turning Speed	0.440	0.710	1.040	1.200	1.410	1.840
Advance (body length)	122.0	146.8	161.4	162.5	164.6	165.6
Transfer (body length)	121.0	145.5	160.5	161.3	163.6	164.6
Tactical Diameter (body length)	244.2	295.5	326.4	326.4	331.5	334.7
Time to 180 turn (s)	751.5	566.6	444.0	367.8	340.0	256.6
Average Turn Rate (deg/s)	0.24	0.32	0.41	0.49	0.53	0.70
Omega 2 (RPM)	3000	3000	3000	3000	3000	3000
Omega 1 (RPM)	250	250	250	250	250	250
Omega Diff (RPM)	2750	2750	2750	2750	2750	2750
Avg RPM	1625	1625	1625	1625	1625	1625

No Speed Control – Shrouded Propeller

Shrouded

Prop Size (body radius)	0.595	0.629	0.670
Omega Diff (RPM)	2750	2750	2750
Best Turning Speed	1.46	1.67	1.95
Advance (body length)	190.3	188.3	188.4
Transfer (body length)	189.4	187.2	187.5
Tactical Diameter (body length)	383.0	379.7	380.8
Time to 180 turn (s)	264.9	309.5	281.9
Average Turn Rate (deg/s)	0.68	0.58	0.64
Omega 2 (RPM)	3000	3000	3000
Omega 1 (RPM)	250	250	250
Omega Diff (RPM)	2750	2750	2750
Avg RPM	1625	1625	1625

No Speed Control – Unshrouded vs. Shrouded

	Unshrouded	Shrouded	
Prop Size (cm)	0.629	0.629	Percent Difference
Omega Diff (RPM)	2750	2750	N/A
Best Turning Speed	1.50	1.50	N/A
Advance (body length)	253.4	152.1	-39.98
Transfer (body length)	252.6	150.9	-40.28
Tactical Diameter (body length)	508.3	306.7	-39.65
Time to 180 turn (s)	448.5	275.0	-38.68
Average Turn Rate (deg/s)	0.40	0.65	63.07
Omega 2 (RPM)	3000	3000	N/A
Omega 1 (RPM)	250	250	N/A
Omega Diff (RPM)	2750	2750	N/A
Avg RPM	1625	1625	N/A

Speed Control – 0.595 Body Radius Propeller No Shroud

Test Speed (m/s)	0.50	0.75	1.00	1.25	1.50	1.75	2.00	2.25
Advance (body length)	665.9	815.5	914.7	1115	1283	1798	2713	4069
Transfer (body length)	665.7	815.2	914.4	1106	1266	1767	2638	4087
Tactical Diameter (body length)	1343	1629	1837	2230	2564	3297	5428	8130
Time to 180 turn (s)	3240	2665	2354	2224	2104	2556	3270	4500
Average Turn Rate (deg/s)	0.06	0.07	0.08	0.08	0.09	0.07	0.06	0.04
Omega 2 (RPM)	1222	1640	1837	2470	2884	3000	3000	3000
Omega 1 (RPM)	250	250	250	876	1281	1586	1841	2065
Omega Diff (RPM)	972	1390	1587	1594	1603	1414	1159	935
Avg RPM	736	945	1044	1673	2083	2293	2421	2533

Speed Control – 0.595 Body Radius Propeller Shroud

Test Speed (m/s)	0.50	0.75	1.00	1.25	1.50	1.75	2.00	2.25	2.50
Advance (body length)	628.4	788.1	898.6	979.6	1083.	1256	1384	1704	2328
Transfer (body length)	628.4	787.8	898.3	979.3	994.7	1345	1515	1729	2308
Tactical Diameter (body length)	1267	1596	1820	1975	2173	2518	2779	3408	4657
Time to 180 turn (s)	3041	2563	2204	1952	1764	1744.	1684	1846	2300.0
Average Turn Rate (deg/s)	0.06	0.07	0.08	0.09	0.10	0.10	0.11	0.10	0.08
Omega 2 (RPM)	984	1300	1613	1924	2234	2543	2852	3000	3000
Omega 1 (RPM)	250	250	250	250	518	960	1255	1492	1697
Omega Diff (RPM)	734	1050	1363	1674	1716	1583	1597	1508	1303
Avg RPM	617	775	932	1087	1376	1752	2054	2246	2349

Speed Control – 0.629 Body Radius Propeller No Shroud

Test Speed (m/s)	0.50	0.75	1.00	1.25	1.50	1.75	2.00	2.25	2.50
Advance (body length)	652.3	794.2	889.1	975.6	1165	1301	1764	2528	3604
Transfer (body length)	652.3	793.9	888.8	1037	1210	1329	1766	2420	3516
Tactical Diameter (body length)	1325	1587	1776	1956	2331	2601	3524	5061	7210
Time to 180 turn (s)	3199	2603	2201	2017	1885	1810	2172	2855	3610
Average Turn Rate (deg/s)	0.06	0.07	0.08	0.09	0.10	0.10	0.08	0.06	0.05
Omega 2 (RPM)	1080	1450	1817	2183	2548	2912	3000	3000	3000
Omega 1 (RPM)	250	250	250	400	964	1304	1571	1800	2002
Omega Diff (RPM)	830	1200	1567	1783	1584	1608	1429	1200	998
Avg RPM	665	850	1034	1292	1756	2108	2286	2400	2501

Speed Control -- 0.629 Body Radius Propeller Shroud

Test Speed (m/s)	0.50	0.75	1.00	1.25	1.50	1.75	2.00	2.25	2.50
Advance (body length)	719.6	853.6	946.5	1015	1067	1138	1292	1409	1520
Transfer (body length)	719.0	853.3	946.2	1014	1066	1190	1325	1492	1624
Tactical Diameter (body length)	1447	1725	1892	2028	2133	2278	2584	2821	3045
Time to 180 turn (s)	3476	2769	2298	1973	1731	1620	1568	1501	1484
Average Turn Rate (deg/s)	0.05	0.07	0.08	0.09	0.10	0.11	0.11	0.12	0.12
Omega 2 (RPM)	813	1095	1373	1649	1923	2198	2471	2745	3000
Omega 1 (RPM)	250	250	250	250	250	438	877	1160	1387
Omega Diff (RPM)	563	845	1123	1399	1673	1760	1594	1585	1613
Avg RPM	532	673	812	950	1087	1318	1674	1953	2194

Speed Control – 0.670 Body Radius Propeller No Shroud

Test Speed (m/s)	0.50	0.75	1.00	1.25	1.50	1.75	2.00	2.25	2.50
Advance (body length)	637.7	768.5	857.2	921.3	1010	1165	1278	1559	2179
Transfer (body length)	637.4	768.5	856.9	921	1032	1166	1343	1653	2251
Tactical Diameter (body length)	1297	1578	1764	1840	2019	2328	2258	3178	4361
Time to 180 turn (s)	3118.	2535	2160	1744	1654	1611	1523	1688	2196
Average Turn Rate (deg/s)	0.06	0.07	0.08	0.10	0.11	0.11	0.12	0.11	0.08
Omega 2 (RPM)	944	1269	1590	1910	2228	2547	2864	3000	3000
Omega 1 (RPM)	250	250	250	250	507	963	1265	1507	1715
Omega Diff (RPM)	694	1019	1340	1660	1721	1584	1599	1493	1285
Avg RPM	597	759	920	1080	1368	1755	2065	2253	2358

Speed Control – 0.670 Body Radius Propeller Shroud

Test Speed (m/s)	0.50	0.75	1.00	1.25	1.50	1.75	2.00	2.25	2.50
Advance (body length)	716.1	832.5	916.4	979.3	1028	1067	1107	1240	1353
Transfer (body length)	716.1	832.2	916.1	979.0	1028	1066	1016	1368	1422
Tactical Diameter (body length)	1440	1664	1863	1958	2055	2133	2222	2492	2709
Time to 180 turn (s)	3467	2690	2242	1876	1642	1483	1363	1347	1296
Average Turn Rate (deg/s)	0.05	0.07	0.08	0.10	0.11	0.12	0.13	0.13	0.14
Omega 2 (RPM)	710	958	1201	1442	1683	1922	2161	2400	2638
Omega 1 (RPM)	250	250	250	250	250	250	340	786	1059
Omega Diff (RPM)	460	708	951	1192	1433	1672	1821	1614	1579
Avg RPM	480	604	726	846	967	1086	1251	1593	1849

Speed Control – 0.744 Body Radius Propeller No Shroud

Test Speed (m/s)	0.50	0.75	1.00	1.25	1.50	1.75	2.00	2.25	2.50
Advance (body length)	628.4	735.4	811.3	867.6	910.9	945.3	1031	1146	1235
Transfer (body length)	628.3	735.1	811.0	867.3	910.6	945.0	1107	1174	1206
Tactical Diameter (body length)	1277	1516	1621	1734	1821	1888	2065	2294	2470
Time to 180 turn (s)	3046	2400	1932	1697	1488	1277	1221	1301	1200
Average Turn Rate (deg/s)	0.06	0.07	0.09	0.11	0.12	0.14	0.15	0.14	0.15
Omega 2 (RPM)	748	1009	1265	1520	1773	2026	2279	2531	2782
Omega 1 (RPM)	250	250	250	250	250	250	602	946	1194
Omega Diff (RPM)	498	759	1015	1270	1523	1776	1677	1585	1588
Avg RPM	499	630	758	885	1012	1138	1441	1739	1988

Appendix D: Depth changing open loop test data

Fin Actuated

Prop Size (cm)	Fin	Fin	Fin	Fin	Fin
Test Speed (m/s)	0.50	1.00	1.50	2.00	2.50
Depth Overshoot (m)	0.00	0.00	0.00	0.00	0.00
Time to change 10m depth	116.1	58.23	39.01	29.37	23.59
Average depth rate (m/s)	0.0862	0.172	0.256	0.340	0.424
Omega 2 (RPM)	N/A	N/A	N/A	N/A	N/A
Omega 1 (RPM)	N/A	N/A	N/A	N/A	N/A
Omega Diff (RPM)	N/A	N/A	N/A	N/A	N/A
Avg RPM	N/A	N/A	N/A	N/A	N/A

No Speed Control Unshrouded

Prop Size (Body Radius)	0.446	0.521	0.595	0.629	0.670	0.744
Omega Diff (RPM)	2750	2750	2750	2750	2750	2750
Best Operating Speed	0.440	0.710	1.04	1.20	1.41	1.84
Depth Overshoot (m)	0.866	0.989	0.982	0.923	0.851	0.663
Time to change 10m depth	882.	623.8	451.8	390.5	331.4	243.9
Average depth rate (m/s)	0.01133	0.01603	0.02213	0.02561	0.03018	0.04100
Omega 2 (RPM)	3000	3000	3000	3000	3000	3000
Omega 1 (RPM)	250	250	250	250	250	250
Omega Diff (RPM)	2750	2750	2750	2750	2750	2750
Avg RPM	1625	1625	1625	1625	1625	1625

No Speed Control Shrouded

Prop Size (Body Radius)	0.595	0.629	0.670
Omega Diff (RPM)	2750	2750	2750
Best Operating Speed	1.46	1.67	1.95
Depth Overshoot (m)	1.06	0.96	0.85
Time to change 10m depth	359.1	308.5	259.8
Average depth rate (m/s)	0.02785	0.03241	0.03849
Omega 2 (RPM)	3000	3000	3000
Omega 1 (RPM)	250	250	250
Omega Diff (RPM)	2750	2750	2750
Avg RPM	1625	1625	1625

Speed Control – 0.595 Body Radius Propeller No Shroud

Test Speed (m/s)	0.50	0.75	1.00	1.25	1.50	1.75	2.00	2.25
Depth Overshoot (m)	1.57	3.04	4.5	5.77	5.16	5.56	6.84	6.62
Time to change 10m depth	639.8	539.9	591.9	624.7	513.3	539.4	756.7	834.9
Average depth rate (m/s)	0.0156299	0.018523	0.0168947	0.016009	0.0194803	0.018539	0.01321528	0.01197777
Omega 2 (RPM)	1222	1640	2039	2470	2884	3000	3000	3000
Omega 1 (RPM)	250	250	250	876	1281.00	1586.00	1841.00	2065.00
Omega Diff (RPM)	972.00	1390.00	1789.00	1594.00	1603.00	1414.00	1159.00	935.00
Avg RPM	736.00	945.00	1144.50	1673.00	2082.50	2293.00	2420.50	2532.50

85

Speed Control – 0.595 Body Radius Propeller Shroud

Test Speed (m/s)	0.50	0.75	1.00	1.25	1.50	1.75	2.00	2.25	2.50
Depth Overshoot (m)	1.35	2.26	3.47	4.58	5.47	5.94	5.49	5.84	6.35
Time to change 10m depth	508.3	461	488.4	481.8	504.5	475.1	411.7	422.1	486.7
Average depth rate (m/s)	0.01967	0.02169	0.02048	0.02076	0.01982	0.02105	0.02429	0.02369	0.02055
Omega 2 (RPM)	985	1300	1613	1924	2234	2543	2840	3000	3000
Omega 1 (RPM)	250	250	250	250	518	960	1244	1492	1697
Omega Diff (RPM)	735	1050	1363	1674	1716	1583	1596	1508	1303
Avg RPM	618	775	932	1087	1376	1752	2042	2246	2349

Speed Control – 0.629 Body Radius Propeller No Shroud

Test Speed (m/s)	0.50	0.75	1.00	1.25	1.50	1.75	2.00	2.25	2.50
Depth Overshoot (m)	1.34	2.39	3.77	5.03	5.71	5.18	5.53	5.41	6.67
Time to change 10m depth	597.1	520.7	548.6	497.6	526.3	451.3	471.7	997.4	713.2
Average depth rate (m/s)	0.01675	0.01920	0.01822	0.02010	0.01900	0.02216	0.02120	0.01003	0.01402
Omega 2 (RPM)	1065	1450	1817	2197	2548	2897	3000	3000	3000
Omega 1 (RPM)	250	250	250	437	964	1292	1562	1800	2010
Omega Diff (RPM)	815	1200	1567	1760	1584	1605	1438	1200	990
Avg RPM	658	850	1034	1317	1756	2095	2281	2400	2505

98

Speed Control – 0.629 Body Radius Propeller Shroud

Test Speed (m/s)	0.50	0.75	1.00	1.25	1.50	1.75	2.00	2.25	2.50
Depth Overshoot (m)	1.47	1.97	2.84	3.83	4.72	5.46	6.08	5.48	5.66
Time to change 10m depth	479.3	437.1	403.0	448.0	428.9	443.9	436.0	367.5	361.8
Average depth rate (m/s)	0.02086	0.02288	0.02481	0.02232	0.02332	0.02253	0.02294	0.02721	0.02764
Omega 2 (RPM)	813	1095	1373	1649	1923	2198	2471	2745	3000
Omega 1 (RPM)	250	250	250	250	250	438	877	1160	1387
Omega Diff (RPM)	563	845	1123	1399	1673	1760	1594	1585	1613
Avg RPM	532	673	812	950	1087	1318	1674	1953	2194

Speed Control – 0.670 Body Radius Propeller No Shroud

Test Speed (m/s)	0.50	0.75	1.00	1.25	1.50	1.75	2.00	2.25	2.50
Depth Overshoot (m)	1.29	1.88	2.96	4.08	5.13	5.64	5.17	5.44	5.86
Time to change 10m depth	543.7	490.47	427.1	471.2	472.5	451.6	392.1	404.1	428.1
Average depth rate (m/s)	0.01839	0.02039	0.02341	0.02122	0.02116	0.02214	0.02550	0.024746	0.02336
Omega 2 (RPM)	944	1269	1590	1897	2228	2547	2864	3000	3000
Omega 1 (RPM)	250	250	250	250	507	963	1265	1516	1715
Omega Diff (RPM)	694	1019	1340	1647	1721	1584	1599	1484	1285
Avg RPM	597	760	920	1074	1368	1755	2065	2258	2358

87

Speed Control – 0.670 Body Radius Propeller Shroud

Test Speed (m/s)	0.50	0.75	1.00	1.25	1.50	1.75	2.00	2.25	2.50
Depth Overshoot (m)	1.56	1.79	2.34	3.12	3.95	4.69	5.32	5.9	5.51
Time to change 10m depth	447.7	402.6	374.2	345.1	388.8	372.7	345.4	382	327.2
Average depth rate (m/s)	0.02234	0.02484	0.02672	0.02898	0.02572	0.02683	0.02895	0.026178	0.03056
Omega 2 (RPM)	710	958	1201	1443	1683	1922	2161	2400	2638
Omega 1 (RPM)	250	250	250	250	250	250	340	786	1059
Omega Diff (RPM)	460	708	951	1193	1433	1672	1821	1614	1579
Avg RPM	480	604	726	847	967	1086	1251	1593	1849

Speed Control – 0.744 Body Radius Propeller No Shroud

Test Speed (m/s)	0.50	0.75	1.00	1.25	1.50	1.75	2.00	2.25	2.50
Depth Overshoot (m)	1.36	1.65	2.25	3.11	3.99	4.75	5.43	5.64	5.28
Time to change 10m depth	439.1	395.3	363.3	331.4	372.5	353.9	372.0	350.0	308.8
Average depth rate (m/s)	0.02277	0.02530	0.02752	0.03018	0.02685	0.02826	0.02688	0.02858	0.03239
Omega 2 (RPM)	748	1009	1265	1520	1773	2026	2279	2531	2782
Omega 1 (RPM)	250	250	250	250	250	250	602	946	1194
Omega Diff (RPM)	498	759	1015	1270	1523	1776	1677	1585	1588
Avg RPM	499	630	758	885	1012	1138	1441	1739	1988

Appendix E: Surge velocity changing open loop test data

0.446 Body Radius Propeller Unshrouded

Desired Speed Setting (m/s)	Final Speed (m/s)	Percent Lost	RPM
0.50	0.248	50.40%	1132
1.00	0.603	39.70%	1787
1.50	0.928	38.13%	2573
1.75	1.09	37.71%	2965
2.00	1.03	48.50%	3000
Assess Max Speed	1.09		

0.521 Body Radius Propeller Unshrouded

Desired Speed Setting (m/s)	Final Speed (m/s)	Percent Lost	RPM
0.50	0.297	40.60%	915
1.00	0.688	31.20%	1404
1.50	1.05	30.00%	2013
1.75	1.42	29.00%	2618
2.00	1.60	28.89%	2915
2.50	1.57	37.20%	3000
Assess Max Speed	1.60		

0.595 Body Radius Propeller Unshrouded

Desired Speed Setting (m/s)	Final Speed (m/s)	Percent Lost	RPM
0.50	0.335	33.00%	745
1.00	0.751	24.90%	1122
1.50	1.14	24.00%	1606
2.00	1.54	23.00%	2086
2.50	1.93	22.80%	2556
2.75	2.13	22.55%	2778
3.00	2.30	23.33%	3000
Assess Max Speed	2.30		

0.595 Body Radius Propeller Shrouded

Desired Speed Setting (m/s)	Final Speed (m/s)	Percent Lost	RPM
0.50	0.366	26.80%	601
1.00	0.801	19.90%	895
1.50	1.22	18.67%	1278
2.00	1.63	18.50%	1658
2.50	2.05	18.00%	2031
3.00	2.47	17.67%	2397
3.50	2.89	17.43%	2758
3.75	3.10	17.33%	2937
4.00	3.07	23.25%	3000
Assess Max Speed	3.10		

0.629 Body Radius Propeller Unshrouded

Desired Speed Setting (m/s)	Final Speed (m/s)	Percent Lost	RPM
0.50	0.349	30.20%	680
1.00	0.774	22.60%	1019
1.50	1.18	21.33%	1457
2.00	1.58	21.00%	1891
2.50	1.99	20.40%	2317
3.00	2.39	20.33%	2736
3.25	2.60	20.00%	2943
3.50	2.55	27.14%	3000
Assess Max Speed	2.60		

0.629 Body Radius Propeller Shrouded

Desired Speed Setting (m/s)	Final Speed (m/s)	Percent Lost	RPM
0.50	0.379	24.20%	547
1.00	0.820	18.00%	809
1.50	1.24	17.33%	1156
2.00	1.67	16.50%	1499
2.50	2.09	16.40%	1835
3.00	2.52	16.00%	2166
3.50	2.95	15.71%	2492
4.00	3.37	15.75%	2814
4.25	3.59	15.53%	2974
4.50	3.49	22.44%	3000
Assess Max Speed	3.59		

0.670 Body Radius Propeller Unshrouded

Desired Speed Setting (m/s)	Final Speed (m/s)	Percent Lost	RPM
0.50	0.364	27.20%	614
1.00	0.797	20.30%	914
1.50	1.21	19.33%	1306
2.00	1.62	19.00%	1694
2.50	2.04	18.40%	2075
3.00	2.46	18.00%	2449
3.50	2.87	18.00%	2818
3.75	3.08	17.87%	3000
4.00	2.93	26.75%	3000
Assess Max Speed	3.08		

0.670 Body Radius Propeller Shrouded

Desired Speed Setting (m/s)	Final Speed (m/s)	Percent Lost	RPM
0.50	0.391	21.80%	491
1.00	0.839	16.10%	724
1.50	1.27	15.33%	1032
2.00	1.70	15.00%	1339
2.50	2.14	14.40%	1638
3.00	2.57	14.33%	1933
3.50	3.01	14.00%	2224
4.00	3.44	14.00%	2511
4.50	3.88	13.78%	2796
4.75	4.10	13.68%	2937
5.00	4.10	18.00%	3000
Assess Max Speed	4.10		

0.744 Body Radius Propeller Unshrouded

Desired Speed Setting (m/s)	Final Speed (m/s)	Percent Lost	RPM
0.50	0.386	22.80%	512
1.00	0.832	16.80%	756
1.50	1.26	16.00%	1079
2.00	1.69	15.50%	1400
2.50	2.12	15.20%	1713
3.00	2.55	15.00%	2022
3.50	2.98	14.86%	2326
4.00	3.42	14.50%	2627
4.50	3.85	14.44%	2924
4.75	3.88	18.32%	3000
Assess Max Speed	3.88		

Appendix F: Coupled controller analysis data

0.595 Body Radius Propeller No Shroud

Test Speed (m/s)	0.50	0.75	1.00	1.25	1.50	1.75	2.00	2.25
Steady State RPM	882	1173	1464	1756	2047	2338	2630	2921
Advance (Body Length)	1200	1384	1456	1761	1988	2930	4700	7164
Transfer (Body Length)	845.6	995.9	1080	1302	1480	2083	3159	4665
Tactical Diameter (Body Length)	1522	1828	2000.	2418	2763	3882	5874	8735
Time to 180 turn (s)	4118	3298	2750	2615	2494	3036	4100.	5507
Average Turn Rate (deg/s)	0.04	0.05	0.07	0.07	0.07	0.06	0.04	0.03
Depth Overshoot (m)	6.46	6.56	6.46	6.74	6.86	7.65	8.41	8.84
Time to change 10m depth	1354	1003	777.2	717.1	653.2	852.2	1184	1561.2
Average depth rate (m/s)	0.007	0.010	0.013	0.014	0.015	0.012	0.008	0.006
Omega 2 (RPM)	1222	1640	2056	2470	2884	3000	3000	3000
Omega 1 (RPM)	250	250	250	876	1281	1586	1841	2065
Omega Diff (RPM)	972	1390	1806	1594	1603	1414	1159	935
Avg RPM	624	829	1036	1310	1578	1697	1760	1821

0.595 Body Radius Propeller Shroud

Test Speed (m/s)	0.50	0.75	1.00	1.25	1.50	1.75	2.00	2.25	2.50
Steady State RPM	718	936	1154	1372	1589	1807	2025	2242	2460
Advance (Body Length)	1108	1319	1424	1478	1590	1828	1986	2497	3615
Transfer (Body Length)	791.2	956.8	1059	1130	1235	1419	1554	1909	2627
Tactical Diameter (Body Length)	1432	1768	1986	2129	2322	2679	2944	3614	4957
Time to 180 turn (s)	3833	3125	2620	2271	2071	2043	1962	2159	2701
Average Turn Rate (deg/s)	0.05	0.06	0.07	0.08	0.09	0.09	0.09	0.08	0.07
Depth Overshoot (m)	6.25	6.43	6.39	6.27	6.27	6.47	6.54	6.99	7.76
Time to change 10m depth	1272	966.2	761.3	614.2	510.6	516.2	480.1	511.8	691.6
Average depth rate (m/s)	0.008	0.010	0.013	0.016	0.020	0.019	0.021	0.020	0.014
Omega 2 (RPM)	985	1300	1613	1924	2234	2543	2852	3000	3000
Omega 1 (RPM)	250	250	250	250	518	960	1255	1492	1697
Omega Diff (RPM)	735	1050	1363	1674	1716	1583	1597	1508	1303
Avg RPM	508	662	816	970	1147	1359	1558	1675	1723

0.629 Body Radius Propeller No Shroud

Test Speed (m/s)	0.50	0.75	1.00	1.25	1.50	1.75	2.00	2.25	2.50
Steady State RPM	784	1040	1297	1553	1810	2067	2323	2580	2836
Advance (Body Length)	1168	1334	1404	1474	1743	1907	2729	4173	6155
Transfer (Body Length)	826.5	965.9	1048	1127	1330	1469	2009	2906	4121
Tactical Diameter (Body Length)	1490	1781	1956	2105	2496	2770	3773	5437	7728
Time to 180 turn (s)	4004	3158	2607	2252	2228	2115	2552	3344	4339
Average Turn Rate (deg/s)	0.04	0.06	0.07	0.08	0.08	0.09	0.07	0.05	0.04
Depth Overshoot (m)	6.38	6.46	6.35	6.26	6.52	6.59	7.35	8.13	8.64
Time to change 10m depth	1325	974.5	751.7	612	586.6	536.9	661.6	910.7	1203
Average depth rate (m/s)	0.008	0.010	0.013	0.016	0.017	0.019	0.015	0.011	0.008
Omega 2 (RPM)	1080	1450	1817	2183	2548	2912	3000	3000	3000
Omega 1 (RPM)	250	250	250	400	964	1304	1571.4	1800	2002
Omega Diff (RPM)	830	1200	1567	1783	1584	1608	1429	1200	998
Avg RPM	554	736	917	1110	1362	1595	1693	1749	1803

0.629 Body Radius Propeller Shroud

Test Speed (m/s)	0.50	0.75	1.00	1.25	1.50	1.75	2.00	2.25	2.50
Steady State RPM	602	794	987	1179	1372	1564	1756	1949	2141
Advance (Body Length)	1326	1471	1529	1548	1550	1592	1802	1942	2069
Transfer (Body Length)	919.0	1047	1123	1174	1210	1270	1436	1558	1672
Tactical Diameter (Body Length)	1647	1922	2103	2225	2301	2409	2729	2969	3195
Time to 180 turn (s)	4466	3423	2777	2331	2026	1825	1801	1742	1686
Average Turn Rate (deg/s)	0.04	0.05	0.06	0.08	0.09	0.10	0.10	0.10	0.11
Depth Overshoot (m)	6.73	6.72	6.58	6.40	6.20	6.11	6.28	6.34	6.38
Time to change 10m depth	1561	1110	807.8	643.6	501.2	438.9	419.6	393.8	371.2
Average depth rate (m/s)	0.006	0.009	0.012	0.016	0.020	0.023	0.024	0.025	0.027
Omega 2 (RPM)	813	1095	1373	1649	1923	2198	2471	2745	3000
Omega 1 (RPM)	250	250	250	250	250	438	877	1160	1387
Omega Diff (RPM)	563	845	1123	1399	1673	1760	1594	1585	1613
Avg RPM	425	562	698	834	970	1121	1311	1490	1653

0.670 Body Radius Propeller No Shroud

Test Speed (m/s)	0.50	0.75	1.00	1.25	1.50	1.75	2.00	2.25	2.50
Steady State RPM	691	914	1138	1362	1586	1809	2033	2257	2481
Advance (Body Length)	1132	1273	1339	1358	1435	1646	1778	2268	3327
Transfer (Body Length)	804.9	929.5	1008	1056	1137	1304	1421	1767.	2454
Tactical Diameter (Body Length)	1454	1722	1895	1998	2147	2469	2701	3357	4635
Time to 180 turn (s)	3903	3033	2502	2111	1893	1867	1777	1976	2515
Average Turn Rate (deg/s)	0.05	0.06	0.07	0.09	0.10	0.10	0.10	0.09	0.07
Depth Overshoot (m)	6.30	6.34	6.22	6.04	6.00	6.19	6.24	6.75	7.57
Time to change 10m depth	1293	939.1	718.0	546.0	473.7	449.0	415.7	475.0	639.0
Average depth rate (m/s)	0.008	0.011	0.014	0.018	0.021	0.022	0.024	0.021	0.016
Omega 2 (RPM)	944	1269	1590	1910	2228	2547	2864	3000	3000
Omega 1 (RPM)	250	250	250	250	507	963	1265	1507	1715
Omega Diff (RPM)	694	1019	1340	1660	1721	1584	1599	1493	1285
Avg RPM	488	647	805	963	1142	1361	1565	1679	1728

0.670 Body Radius Propeller Shroud

Test Speed (m/s)	0.50	0.75	1.00	1.25	1.50	1.75	2.00	2.25	2.50
Steady State RPM	532	700	868	1035	1203	1371	1538	1706	1874
Advance (Body Length)	1318	1423	1460	1477	1469	1465	1479	1651	1776
Transfer (Body Length)	914.2	1019	1082	1130	1159	1187	1224	1366	1477
Tactical Diameter (Body Length)	1638	1874	2035	2156	2233	2284	2335	2612	2831
Time to 180 turn (s)	4441	3328	2668	2239	1921	1694	1540	1517	1480
Average Turn Rate (deg/s)	0.04	0.05	0.07	0.08	0.09	0.11	0.12	0.12	0.12
Depth Overshoot (m)	6.72	6.63	6.46	6.27	6.07	5.88	5.76	5.92	5.99
Time to change 10m depth	1553	1026	778.9	613.9	482.6	410.1	357.9	348.1	331.4
Average depth rate (m/s)	0.006	0.010	0.013	0.016	0.021	0.024	0.028	0.029	0.030
Omega 2 (RPM)	710	958	1201	1443	1683	1922	2161	2400	2638
Omega 1 (RPM)	250	250	250	250	250	250	340	786	1059
Omega Diff (RPM)	460	708	951	1193	1433	1672	1821	1614	1579
Avg RPM	376	495	613	732	851	969	1094	1263	1421

0.744 Body Radius Propeller No Shroud

Test Speed (m/s)	0.50	0.75	1.00	1.25	1.50	1.75	2.00	2.25	2.50
Steady State RPM	557	735	912	1089	1266	1444	1621	1798	1975
Advance (Body Length)	1108	1203	1243	1252	1256	1251	1345	1484	1580
Transfer (Body Length)	791.0	887.1	948.4	988.2	1021	1044	1132	1251	1341
Tactical Diameter (Body Length)	1431	1649	1800	1903	1973	2006	2166	2398	2576
Time to 180 turn (s)	3822	2877	2325	1960	1680	1491	1410	1388	1335.
Average Turn Rate (deg/s)	0.05	0.06	0.08	0.09	0.11	0.12	0.13	0.13	0.13
Depth Overshoot (m)	6.25	6.18	6.01	5.82	5.63	5.47	5.53	5.65	5.70
Time to change 10m depth	12720	891.5	638.7	512.2	421.0	341.5	316.5	302.0	285.4
Average depth rate (m/s)	0.008	0.011	0.016	0.020	0.024	0.029	0.032	0.033	0.035
Omega 2 (RPM)	747.7	1008.5	1265	1520	1773	2026	2279	2531	2782
Omega 1 (RPM)	250	250	250	250	250	250	602	946	1194
Omega Diff (RPM)	498	759	1015	1270	1523	1776	1677	1585	1588
Avg RPM	394	520	645	770	895	1021	1179	1351	1514

BIBLIOGRAPHY

- [1] G. Asaamoning, P. Mendes, D. Rosário, and E. Cerqueira. “Drone Swarms as Networked Control Systems by Integration of Networking and Computing.” *Sensors* , vol. 21, no. 2642, April 2021. doi: <https://doi.org/10.3390/s21082642>. Accessed 13 Feb 2024.
- [2] “Asymmetric Propulsion.” Armada Marine Robotics. <https://www.armadamarinerobotics.com/technology> (accessed April 03, 2024).
- [3] P. Cardenas and E. A. de Barros, “Estimation of AUV Hydrodynamic Coefficients Using Analytical and System Identification Approaches”, *IEEE Journal of Ocean Engineering*, Vol 45, No. 4, pp. 1157- 1176, Oct. 2020. Accessed 12 Sept. 2022.
- [4] R. B. Carelli, “Use of an Asymmetric Propeller for Unmanned Underwater Vehicles,” M. S. Thesis, Dept. Mechanical Engineering, Massachusetts Institute of Technology, Cambridge, MA, USA, 2019.
- [5] P. Chiacchio, S. Chiaverini, L. Sciavicco, and B. Siciliano, “Closed-Loop Inverse Kinematics Schemes for Constrained Redundant Manipulators with Task Space Augmentation and Task Priority Strategy,” *The International Journal of Robotics Research*, vol. 10,no. 4, pp. 410-425, August 1991. Accessed 17 July 2023.
- [6] J. R. Cares and J. Q. Dickman Jr., *Operations Research for Unmanned Systems*. Chichester, UK, Hoboken, NJ, USA: Wiley & Sons, Ltd. 2016.
- [7] T. I. Fossen, *Handbook of Marine Craft Hydrodynamics and Motion Control*, 2nd ed. Hoboken, NJ, USA: John Wiley & Sons Ltd, 2021.

- [8] S. Ghosh, "Understanding the Different Types of Manoeuvres of a Vessel." Marine Insight. <https://www.marineinsight.com/naval-architecture/different-types-of-manoevres-of-a-vessel/> (Accessed 19 Mar 2024).
- [9] J. Gruzling. "The development and application of high efficiency nozzles and rudder," *Transactions-Society of Naval Architects and Marine Engineers*. 2011. Accessed 20 March 2024.
- [10] J. Kaeli, R. Littlefield and F. Jaffre, "Asymmetric Propulsion: Thrust and Maneuverability from a Single Degree of Freedom," *OCEANS 2019 MTS/IEEE SEATTLE*, Seattle, WA, USA, 2019, pp. 1-6, doi: 10.23919/OCEANS40490.2019.8962639.
- [11] M. E. Kepler, S. Pawar, D. J. Stilwell, S. Brizzolara and W. L. Neu, "Assessment of AUV Hydrodynamic Coefficients from Analytic and Semi-Empirical Methods," *OCEANS 2018 MTS/IEEE Charleston*, Charleston, SC, USA, 2018, pp. 1-9, doi: 10.1109/OCEANS.2018.8604584.
- [12] R. H. Littlefield, F. Jaffre and J. W. Kaeli, "AUV Propulsion and Maneuvering by Means of Asymmetric Thrust," *2018 IEEE/OES Autonomous Underwater Vehicle Workshop (AUV)*, Porto, Portugal, 2018, pp. 1-6, doi: 10.1109/AUV.2018.8729727.
- [13] G. McCarthy. "HII Unveils REMUS 620 Unmanned Underwater Vehicle." Huntington Ingalls Industries Newsroom. <https://hii.com/news/hii-unveils-remus-620-unmanned-underwater-vehicle/> (accessed April 03, 2024).

- [14] S. W Moore, H. Bohm, and V. Jensen, *Underwater Robotics Science, Design, & Fabrication*. MATE Inspiration for Innovation revision. Monterey, CA, USA: MATE Inspiration for Innovation, 2019.
- [15] J. N. Newman, *Marine Hydrodynamics*, 40th anniversary edition. Cambridge, MA, USA. Massachusetts Institute of Technology, 2017.
- [16] G. E. Packard, R. Stokey, R. Christenson, F. Jaffre, M. Purcell and R. Littlefield, "Hull inspection and confined area search capabilities of REMUS autonomous underwater vehicle," *OCEANS 2010 MTS/IEEE SEATTLE*, Seattle, WA, USA, 2010, pp. 1-4, doi: 10.1109/OCEANS.2010.5664593. Accessed 07 May 2022.
- [17] B. T. Phillips, J. Allder, G. Bolan, R. S. Nagle, A. Redington, T. Hellebrekers, J. Borden, N. Pawlenko, and S. Licht. "Additive Manufacturing aboard a moving vessel at sea using passively stabilized stereolithography (SLA) 3D printing," *Additive Manufacturing*, Vol. 31. Nov. 2019, doi: <https://doi.org/10.1016/j.addma.2019.100969>. Accessed 13 Feb 2024.
- [18] B. T. Phillips, S. Licht, K. S. Haiat, J. Bonney, J. Allder, N. Chaloux, R. Shomberg, and T. J. Noyes. "DEEPi: A miniaturized, robust and economical camera and computer system for deep-sea exploration," *DEEP-SEA RESEARCH Part 1: Oceanographic Research Papers*, Vol. 153. Nov. 2019, doi: <https://doi.org/10.1016/j.dsr.2019.103136>. Accessed 13 Feb 2024.
- [19] T. Prestero, "Verification of a Six-Degree of Freedom Simulation Model for the REMUS Autonomous Underwater Vehicle," M. S. thesis, Dept. Mechanical Engineering and Ocean Engineering, Massachusetts Institute of

Technology and Woods Hole Oceanographic Institute, Cambridge, MA, USA, 2001.

[20] C. Roman. (2022). Underwater Positioning [Online]. Available: <https://brightspace.uri.edu/d2l/home/180794>

[21] T. Salumäe, A. Chemori and M. Kruusmaa, "Motion Control of a Hovering Biomimetic Four-Fin Underwater Robot," *IEEE Journal of Oceanic Engineering*, vol. 44, no. 1, pp. 54-71, Jan. 2019, doi: 10.1109/JOE.2017.2774318. Accessed 17 July 2023.

[22] B. Soash. "ROVs: The Swiss Army Knife of the Ocean." Science Friday. <https://www.sciencefriday.com/educational-resources/rovs-swiss-army-knife-ocean/> (accessed April 03, 2024).

[23] M. Starr. "SharkCam provides viral video, 'groundbreaking' information." CNET. <https://www.cnet.com/science/sharkcam-provides-viral-video-groundbreaking-information/> (accessed April 03, 2024).

[24] P. N. N. Thanh, P. M. Tam, H. . and H. P. H. Anh, "A new approach for three-dimensional trajectory control of under-actuated AUVs with model uncertainties," *Ocean Engineering*, vol. 228. Mar. 2021, doi: <https://doi.org/10.1016/j.oceaneng.2021.108951>

[25] K. D. von Ellenrieder, *Control of Marine Vehicles*. Cham, Switzerland: Springer, 2021.

[26] H. Zhang *et al.*, "The general design of a seafloor surveying AUV system," *2013 OCEANS - San Diego*, San Diego, CA, 2013, pp. 1-5, doi: 10.23919/OCEANS.2013.6741116. Accessed 06 May 2023.

[27] R. B. Zubaly, *Applied Naval Architecture*, Reprint. Agleton, PA, USA:
Schiffer Publishing, Ltd, 2015.